Carbon-Based Catalysts for Selective Electrochemical Nitrogen-to-Ammonia Conversion

Zhang, L.-H.; Yu, F.; Shiju, N.R.

DOI
10.1021/acssuschemeng.1c00575

Publication date
2021

Document Version
Final published version

Published in
ACS Sustainable Chemistry & Engineering

ACS Sustainable Chemistry & Engineering

pubs.acs.org/journal/ascecg

Perspective

Carbon-Based Catalysts for Selective Electrochemical Nitrogen-to-Ammonia Conversion

Lu-Hua Zhang, Fengshou Yu,* and N. Raveendran Shiju*

Cite This: *ACS Sustainable Chem. Eng.* 2021, 9, 7687−7703

Read Online

ACCESS | Metrics & More | Article Recommendations

ABSTRACT: Electrochemical nitrogen reduction reaction (NRR) to ammonia (NH_3) driven by renewable electricity is a promising alternative to the current energy-intensive and fossil feedstock-dependent Haber−Bosch (H−B) process. The intrinsic inertness of N_2 molecule and competition of hydrogen evolution reaction (HER) are the primary challenges for NRR. Although transition metal-based electrocatalysts can solve the kinetic limitation of N≡N activation through the π-back-donation process, the d-orbital electrons of transition metal atoms facilitate the formation of a metal-H bond, boosting the undesirable HER. Carbon-based materials featuring tunable electronic structures and facile formation of defects have significantly improved electrocatalytic NRR activity in the past few years. Therefore, a review on state-of-the-art carbon-based catalysts for NRR is timely to provide a summary of recent developments in theoretical and experimental aspects. In this review, various defect engineering strategies for the evolution of the desired carbon-based electrocatalysts are comprehensively summarized. The intrinsic relationships between the structures of the defective carbon materials and NRR performance are also discussed in detail. This review aims to stimulate greater interests for developing more efficient electrocatalysts for NRR in the future.

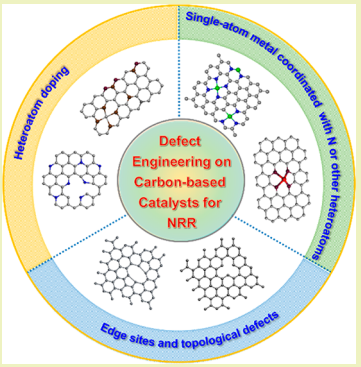

KEYWORDS: *Nitrogen reduction reaction, Electrocatalysis, Carbon-based materials, Defect engineering*

1. INTRODUCTION

In 1909, Fritz Haber invented a process for converting N_2 and H_2 to NH_3 which was rapidly converted to a commercial process by Carl Bosch in 1913.[1] Since then, NH_3 has been widely used in producing nitrogen fertilizers essential for agriculture, resulting in the expansion of the world's population from two to more than seven billion in the last century. Even today, more than 80% of world population benefits indirectly from this conversion process.[2]

For the Haber−Bosch (H−B) technology, the reaction between N_2 and H_2 is carried out under harsh conditions (e.g., 400−600 °C and 20−40 MPa).[3] The high bond energy of N≡N (941 kJ mol^{-1}) in the N_2 molecule results in large energy barriers requiring high temperature for cleaving the triple bond with a reasonable rate.[4] The H−B process is exothermic (ΔH°_{298K} = −45.9 kJ mol^{-1}, ΔG°_{298K} = −16.4 kJ mol^{-1}, K_{eq} = 750), meaning that high temperature is unfavorable for equilibrium shift to NH_3 formation.[5] When the operation temperature is higher than 400 °C at 0.1 MPa, 99% NH_3 is decomposed to N_2 and H_2.[6] Therefore, high pressure is also necessary to get acceptable NH_3 yields. However, even at pressures as high as 40 MPa, the single pass conversion to NH_3 is only 15%. The unconverted H_2 and N_2 are recycled repeatedly, and an eventual conversion efficiency of 97% can be ultimately obtained; however, enormous energy input is necessary to maintain the multistep high temperature and pressure operations.[7] Additionally, H_2 used for NH_3 synthesis is usually produced by highly endothermic reactions from fossil feedstock such as natural gas and petroleum.[3] The harsh reaction conditions and fossil feedstock dependence cause the H−B process to be currently one of the largest energy consumers and greenhouse gas (e.g., CO_2) emitters.[8] Considering the shortage of fossil feedstock and continuous global warming, an environmentally friendly and energy-efficient strategy for reducing N_2 to NH_3 at mild conditions is very much desired.[9]

In the past decades, electrochemical catalysis lying at the heart of several carbon-free energy systems has received great attention,[10−13] opening a new avenue for NH_3 synthesis.[14−27] The chemisorption of reactant on active sites and the subsequent activation process induced by the electron transfer demonstrate an alternative conversion route in which the free energy barrier is low.[28−30] Therefore, enormous efforts have been devoted recently to catalyst design which circumvents the large energy barrier of N_2 reduction. Transition metal-based

Received: January 26, 2021
Revised: April 5, 2021
Published: June 2, 2021

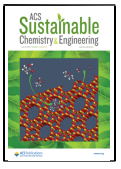

catalysts (e.g., Ru and Mo) have been theoretically predicted to solve the kinetic limitation of N≡N activation through the π-back-donation process.[31−34] Especially, the empty d-orbitals of the transition metals receive the lone-pair electrons from N_2 molecule, and the occupied d-orbitals of transition metal atoms can give electrons to the antibonding orbital of N_2. This weakens the N≡N bond, forming an "acceptance−donation" reaction route. However, the electrons in d-orbital of transition metals can also facilitate the formation of a metal−H bond and therefore can enhance the undesirable side reaction, hydrogen evolution reaction (HER).[35] As a result, the majority of the experimental studies of transition metal-based catalysts show NH_3 producing rates below 10^{-8} mol cm^{-2} s^{-1} and faradaic efficiencies (FEs) lower than 10%, which is far from the threshold needed for practical application in industry.[36,37] According to the suggestions from Giddey et al., an NH_3 formation rate near 10^{-6} mol cm^{-2} s^{-1} and FE more than 50% would be reasonable for practical applications.[38] Therefore, further advances are needed to explore new active catalysts that allow for a large variation in the electronic structure enabling satisfactory catalytic performance.

Carbon-based nanomaterials, especially sp^2-hybridized carbon nanomaterials, have occupied a dominant position in electrocatalysis applications benefiting from their superior electric conductivity, excellent mechanical properties, and high specific surface areas. For nanostructured sp^2 carbon, the basal planes, assembled by sp^2-bonded carbon atoms arranged in a honeycomb lattice are low active centers for chemisorption of the reactants or reaction intermediate. High energy sites are located at the edge of the basal planes of carbon atoms. These sites are associated with high concentrations of unpaired electrons and can be saturated by hydrogen atoms or by heteroatoms, serving as active sites for the activation or dissociation of adsorbing reactants. If the graphitic sheets contain nonhexagonal (such as pentagonal, heptagonal, or octagonal) defects, the additional charge present in such defects can promote the conversion of adsorbed molecules and increase the poor reactivity of the basal plane. In the nanocarbons with well-defined crystal structures, the edge area and defect units are small compared to that of the basal plane in the graphitic structure. Therefore, these materials usually do not exhibit significant catalytic activity for heterogeneous catalysis, which necessitates the engineering of defects to make them active.[39−42]

Doping with heteroatoms, creating topological and defects edge sites, and surface functionalization have been widely used to facilitate the electrochemical performance of carbon-based catalysts for a couple of energy conversion reactions (e.g., HER, oxygen reduction reaction (ORR), oxygen evolution reaction (OER), and carbon dioxide reduction reaction (CO_2RR).[43−47] In one of our previous reviews, the types of catalytic sites for several mainstream nanocarbons were discussed in detail. It was shown that, by properly tuning the electronic structure and or geometric morphology of the nanocarbon catalysts, the activation and/or dissociation of adsorbing molecules on basal planes of the graphitic sheets are optimized, resulting in improved electrocatalytic performance.[43]

Following these early studies, carbon-based materials are rationally expected to enhance electrocatalytic nitrogen reduction reaction (NRR) activity and extensive research has been carried out recently. However, the following issues are yet to be addressed: (1) the current research on carbon-based NRR electrocatalysts is fragmented and lacks comprehensive and systematic overview; (2) the structure/composition-performance relationships are not yet well understood and common trends in catalyst design are still not established. Here, we review the state-of-the-art in carbon-based materials for electrochemical NRR, considering various strategies for efficient catalyst design, including heteroatom doping, edge site and topological defect engineering, and single-atom metal coordinated with nitrogen or other heteroatoms in carbon matrix (Figure 1). Importantly, we also summarize the intrinsic

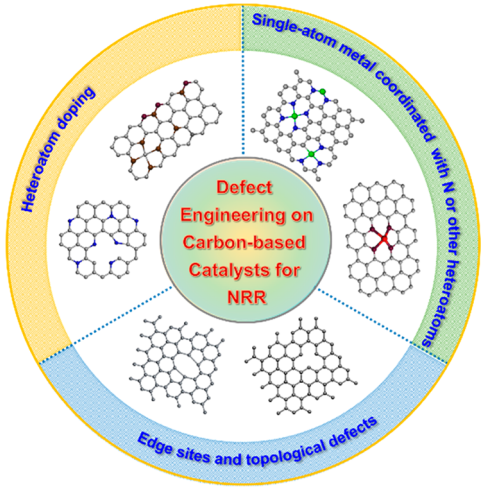

Figure 1. Defect engineering on carbon-based catalysts for electrochemical NRR.

relationships between the structures of defective carbon-based materials and NRR performance using experimental as well as theoretical aspects, and then give a final summary with perspectives on critical challenges and outlooks in the field.

2. FUNDAMENTALS OF ELECTROCHEMICAL NRR

For electrochemical NRR, the N_2 molecule is diffused to the surface of the working electrode and then reduced by electrons with simultaneous proton addition forming NH_3.[48] There are several obviously potential advantages of electrochemical NH_3 synthesis compared to the H−B process. First, the activation of N_2 molecules in this electrochemical cell is driven by electrical energy rather than thermal energy enabling mild operation conditions. Therefore, catalysts with low endurance for high temperature and pressure can be used for electrochemical NRR. Second, the mild liquid-phase reaction conditions enable a great chemical space to optimize catalytic performance by tuning pH, type of electrolyte, and potential range in electrochemical NRR. Third, H_2O rather than H_2 acts as the proton source and the reducing agent during electrochemical NH_3 synthesis, eliminating the dependence on the fossil fuels and reduction of energy input the electrochemical systems can directly use renewable electricity produced from solar or wind sources, enabling decentralized NH_3 production.

Electrochemical NRR is a complex process in gas−liquid−solid three-phase interfaces: N_2 molecules need to diffuse to the working electrode surface first. This should be followed by further reduction by electrons with simultaneous proton addition. However, solubility of N_2 in water is only 0.66 mmol L^{-1} under ambient conditions, which significantly limits NH_3 yields.[19] The following adsorption and activation of N_2

https://doi.org/10.1021/acssuschemeng.1c00575
ACS Sustainable Chem. Eng. 2021, 9, 7687−7703

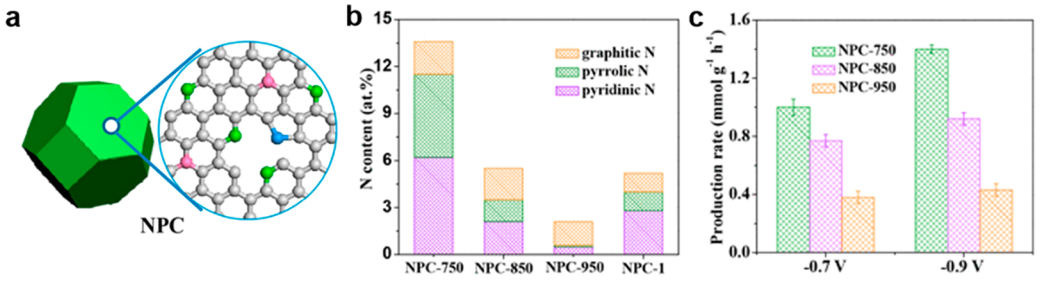

Figure 2. (a) Schematic illustration for NPCs synthesis. (b) Contents of various N species in NPCs. (c) NH_3 formation rates of NPC samples [Reproduced with permission from Figures 1, 5, and 6 in ref 68. Copyright 2018 American Chemical Society].

Table 1. Comparison of Various Carbon-Based Catalysts for NRR

catalyst	electrolyte	FE	NH_3 yield rate	^{15}N isotope	ref
		Heteroatom-Doped Carbons			
N-doped porous carbon	0.05 M H_2SO_4	1.42%	23.8 $\mu g\ h^{-1}\ mg_{cat}^{-1}$	no	68
ZIF-derived N-doped disordered carbon	0.1 M KOH	10.2%	57.8 $\mu g\ h^{-1}\ cm^{-2}$	no	69
N-doped carbon nanospikes (CNS)	0.25 M $LiClO_4$	11.56 ± 0.85%	97.18 ± 7.13 mg $h^{-1}\ cm^{-2}$	yes	72
B-doped graphene	0.05 M H_2SO_4	10.8%	9.8 $\mu g\ h^{-1}\ cm^{-2}$	yes	78
B-doped diamond	0.05 M H_2SO_4 + 0.2 M Li_2SO_4	21.2%	19.1 $\mu g\ h^{-1}\ cm^{-2}$	yes	73
O-doped graphene	M HCl	12.6%	21.3 $\mu g\ h^{-1}\ mg^{-1}$	yes	79
O-carbon nanotube	0.1 M $LiClO_4$	12.50%	32.33 $\mu g\ h^{-1}\ mg_{cat}^{-1}$	yes	80
S-doped graphene	0.1 M HCl	11.5%	27.3 $\mu g\ h^{-1}\ mg_{cat}^{-1}$	no	83
MOF-derived O-doped carbon	0.1 M KOH	1.16%	0.49 $\mu g\ h^{-1}\ cm^{-2}$	yes	84
MOF-derived S-doped carbon	0.1 M KOH	1.48%	0.42 $\mu g\ h^{-1}\ cm^{-2}$	yes	84
MOF-derived Se-doped carbon	0.1 M KOH	3.92%	1.14 $\mu g\ h^{-1}cm^{-2}$	yes	84
MOF-derived Te-doped carbon	0.1 M KOH	4.67%	1.91 $\mu g\ h^{-1}\ cm^{-2}$	yes	84
3D F-doped porous carbon	0.05 M H_2SO_4	54.8%	197.7 $\mu g\ mg_{cat}^{-1}\ h^{-1}$	yes	85
Cl-doped ultrathin graphdiyne	0.1 M HCl	8.7%	10.7 $\mu g\ h^{-1}\ cm^{-2}$	yes	87
P-doped carbon nanotubes	0.25 M $LiClO_4$	12.5%	24.4 $\mu g\ h^{-1}\ mg_{cat}^{-1}$	no	61
P-doped grapheme	0.5 M $LiClO_4$	20.82%	32.33 $\mu g\ h^{-1}\ mg_{cat}^{-1}$	no	62
B, N-codoped porous carbon nanofiber	0.1 M KOH	13.2%	32.5 mg $h^{-1}\ mg_{cat}^{-1}$	yes	93
		Intrinsic Defective Carbons			
defective reduced graphene oxide	0.1 M HCl	22.0%	7.8 $\mu g\ h^{-1}\ mg_{cat}^{-1}$	yes	101
defective reduced graphene oxide	0.1 M KOH	10.8%	7.4 $\mu g\ h^{-1}\ mg_{cat}^{-1}$	yes	101
defect-rich nitrogen-doped carbon	0.1 M KOH	10.2%	3.4 × 10^{-6} mol $cm^{-2}\ h^{-1}$	no	69
		Atomic Metal Species Coordinated Carbons			
Ru SAs/N−C	0.05 M H_2SO_4	29.6%	120.9 $\mu g\ mg_{cat}^{-1}\ h^{-1}$	yes	131
Ru@ZrO_2/NC	0.1 M HCl	21%	3.665 $\mu g\ h^{-1}\ mg_{Ru}^{-1}$	yes	130
Au SAs-NDPCs	0.1 M HCl	12.3%	2.32 $\mu g\ h^{-1}\ cm^{-2}$	no	134
Au_1/C_3N_4	0.05 M H_2SO_4	11.1%	1305 $\mu g\ h^{-1}\ mg_{Au}^{-1}$	no	133
SA-Mo/NPC	0.1 M KOH	14.6 ± 1.6%	34.0 ± 3.6 $\mu g\ mg_{cat}^{-1}\ h^{-1}$	yes	136
ISAS-Fe/NC	0.1 M phosphate buffer	18.6 ± 0.8%	62.9 ± 2.7 $\mu g\ h^{-1}\ mg_{cat}^{-1}$	yes	147
Fe-SAs/LCC	0.1 M KOH	29.3%	32.1 $\mu g\ h^{-1}\ mg_{cat}^{-1}$	yes	146
Fe−$(O-C_2)_4$	0.1 M KOH	29.3%	32.1 $\mu g\ h^{-1}\ mg_{cat}^{-1}$	yes	148
Co/N-doped carbon catalysts	0.1 M KOH	10.1%	5.1 $\mu g\ h^{-1}\ mg_{cat}^{-1}$	no	150
Ni−N_x−C	0.1 M KOH	21 ± 1.9%	85 $\mu g\ cm^{-2}\ h^{-1}$	yes	151
Ni−N_x−C	0.5 M $LiClO_4$	18.5 ± 3%	115 $\mu g\ cm^{-2}\ h^{-1}$	yes	151
Ni−N_x−C	0.1 M HCl	1.3%	60 $\mu g\ cm^{-2}\ h^{-1}$	yes	151
NC−Cu	0.1 M HCl	11.7%	49.3 $\mu g\ h^{-1}\ mg_{cat}^{-1}$	yes	154
NC−Cu	0.1 M KOH	13.8%	53.3 $\mu g\ h^{-1}\ mg_{cat}^{-1}$	yes	154

are regarded as the prerequisite for the electrocatalytic NRR. Unfortunately, due to the chemically intrinsic inertness of N_2 molecule, these processes still face several challenges.[49,50] First, as the major challenge in N≡N dissociation, the cleavage energy of the first bond in N≡N reaches up to 410 kJ mol^{-1}. Second, the N_2 molecule lacks a permanent dipole moment and has a proton affinity of 493.8 kJ mol^{-1}. Besides, high ionization potential (15.84 eV) and the negative electron affinity (−1.90 eV) also reduce its reactivity. Third, the undesired energy gap (10.82 eV) between the highest occupied molecular orbital (HOMO) and the lowest unoccupied molecular orbital (LUMO) obstructs electron transfer during reduction reaction.[4,49] After N_2 adsorption/activation steps, the subsequent reduction reactions involve multiple complicated steps involving electron transfer, hydrogenation, and bond cleavage. Depending on the different sequences of hydrogenation and bond cleavage during the reduction process, two kinds of mechanisms were proposed: (i) the

https://doi.org/10.1021/acssuschemeng.1c00575
ACS Sustainable Chem. Eng. 2021, 9, 7687−7703

dissociative and (ii) the associative pathway. For the dissociative mechanism, the bond cleavage occurs with N_2 adsorption on the catalyst surface prior to hydrogenation and then the adsorbed N atoms independently undergo hydrogenation to form NH_3. For the associative pathway, N_2 molecules are first adsorbed on the catalyst surface, and then the triple bond is successively cleaved with consecutive hydrogenation. Cleavage of the final N−N bond is accompanied by the release of NH_3.[15]

Theoretically, N_2 is expected to be activated and reduced to NH_3, when a relatively negative bias compared to equilibrium potentials for N_2 reduction (0.092 V vs RHE) was added to the electrode (eqs 1 and 3).[37,51,52]

$$N_2(g) + 6H^+(aq) + 6e^- \rightleftharpoons 2NH_3(aq) \quad E^0 = 0.092 \text{ V vs RHE} \tag{1}$$

$$2H^+(aq) + 2e^- \rightleftharpoons H_2(g) \quad E^0 = 0.000 \text{ V vs RHE} \tag{2}$$

$$N_2(g) + 6H_2O(l) + 6e^- \rightleftharpoons 2NH_3(aq) + 6OH^-(aq) \quad E^0 = 0.092 \text{ V vs RHE} \tag{3}$$

$$2H_2O(l) + 2e^- \rightleftharpoons H_2(g) + 2OH^-(aq) \quad E^0 = 0.000 \text{ V vs RHE} \tag{4}$$

However, this equilibrium potential is only the average value for the transfer of six protons and six electrons.[15] The equilibrium potential of the first electron affinity for N_2 can reach up to −2.78 V (eq 5), implying the thermodynamic difficulty of N_2 hydrogenation.[53,54]

$$N_2 + e^- \rightleftharpoons N_2^-(g) \quad E^0 = -2.78 \text{ V vs RHE} \tag{5}$$

Therefore, the N_2 molecule is difficult to activate, and the direct $1 - e^-$ reduction is almost impossible under mild conditions.[50] In comparison, parasitic HER only requires two electrons per H_2 produced in a single half reaction (eqs 2 and 4). As a result, it is favorable for the electrons and protons to combine directly through HER, leading to very low selectivity toward NH_3 (low FE_{NH3}). Therefore, a rational design of carbon-based catalysts for the N_2 adsorption/activation toward enhancing electrocatalytic NRR performance is needed for further progress.

3. HETEROATOM-DOPED CARBONS

Heteroatom doping is a way to replace carbon lattice atoms with heteroatoms (e.g., nitrogen (N), boron (B), oxygen (O), sulfur (S), fluorine (F), and chlorine (Cl)). Due to the various electronegativities between doping heteroatoms and C, the charge density and spin density of C atoms are redistributed induced by heteroatom doping, regulating the sorption behaviors of the reactants, intermediates, and products at specific sites and favoring the electron transfer.[42,55] Heteroatom-doped carbon materials have been extensively explored to boost electrochemical ORR and CO_2RR, and recent research shows that the doping effect can be extended to NRR.[56−62]

3.1. Monodoping. *N-Doping.* Considering that the proton is a Lewis acid and N_2 is a Lewis base, developing a carbon-based electrocatalyst with a Lewis acid site should favor N_2 adsorption and activation while suppressing HER.[63] The N atom possesses a higher electronegativity (3.04) than that of C (2.55), which can withdraw electrons from the adjacent carbons.[64] As such, N-doping induces the charge redistribution and polarization, enabling the enhancement in substrate adsorption and catalytic performance as demonstrated in ORR and CO_2RR.[60,65−67] Inspired by this, a series of N-doped porous carbon catalysts (NPCs) (Figure 2a), obtained by pyrolyzing zeolitic imidazolate framework-8 (ZIF-8), were reported for electrochemical NRR under mild conditions.[68] These N-doped porous carbons possess tunable N contents (from 13.6 to 2.1 at %) and controllable N species at different pyrolysis temperatures (Figure 2b). When used for catalytic reduction of N_2 to NH_3, a maximum FE of 1.42% with an NH_3 production rate of 1.40 mmol h^{-1} g^{-1} at −0.9 V was obtained on the NPC-750 sample with the N content of 13.6 at % (Figure 2c and Table 1). Experiments combined with DFT calculations demonstrated that pyridinic and pyrrolic N are the key active centers for N_2 adsorption and subsequent N≡N cleavage. The preferable pathway for NH_3 synthesis is *N≡N → *NH═NH → *NH_2−NH_2 → 2NH_3. Besides, Wu et al.[69] and Zhang et al.[70] also reported that the pyridinic N in the N-doped carbons are critical sites in NRR which are capable of adsorbing N_2 and subsequently dissociating N≡N for the following protonation process. More interestingly, Wu et al. also found that the presence of Fe in N-doped carbon materials would yield a negative effect on ammonia production and facilitate the HER because of Fe coordination with pyridinic N blocking the active centers for NRR.[69]

Although the active sites for N_2 adsorption/activation are similar in all these N-doped carbons, these catalysts showed distinctly different electrochemical activity. Thus, careful tailoring of geometrical microstructure is important for a specific function in electrocatalytic reactions. For example, three-dimensional porous nanocarbons with hierarchical nanostructure could facilitate the transfer of reactant into and out of the inner microporous network, enhancing the accessibility of reactants to active sites located in the inner pores. Moreover, such microstructure construction strategies are often successful, especially when used in combination with other strategies such as heteroatom doping.[71] For example, an extremely textured catalyst, constituted by N-doped carbon nanospikes (CNS), has been reported for NRR recently.[72] The carbon nanospikes feature a unique physical architecture of abundant-oriented nanospikes (∼50 to 80 nm in length), and each spike consists of layers of carbon terminating with a ∼1 nm wide sharp tip. The maximum NH_3 production rate of 97.18 ± 7.13 mg h^{-1} cm^{-2} was obtained with a FE of 11.56 ± 0.85% at −1.19 V. The electrochemical converting N_2 to the product of NH_3 on the carbon nanospike electrodes likely follows a physical mechanism induced by the special sharp texture, which is different than the mechanism mentioned above for N-doped carbons. More specifically, the surface sharp spikes enrich the electric field at the tips, which facilitates the electrochemical reduction of the dissolved N_2 molecule. The counterions in the electrolyte also play a major role in the reaction rates, with the order of Li^+ > Na^+ > K^+. Simulation revealed a layer of desolvated Li^+ counterions close to the electrode (0.2 nm) which restricts water approach to the electrode surface while allowing N_2 access, promoting NRR with suppressed HER.

B-Doping. Unlike N, B has a smaller electronegativity (2.04) than that of C (2.55) and gets positively charged when doped in the carbon lattice. N_2 is a weak Lewis base, thus, boron with an empty orbital is an ideal Lewis acid site to bind N_2.[73] Simultaneously, the electron-deficient B prevents binding

https://doi.org/10.1021/acssuschemeng.1c00575
ACS Sustainable Chem. Eng. 2021, 9, 7687−7703

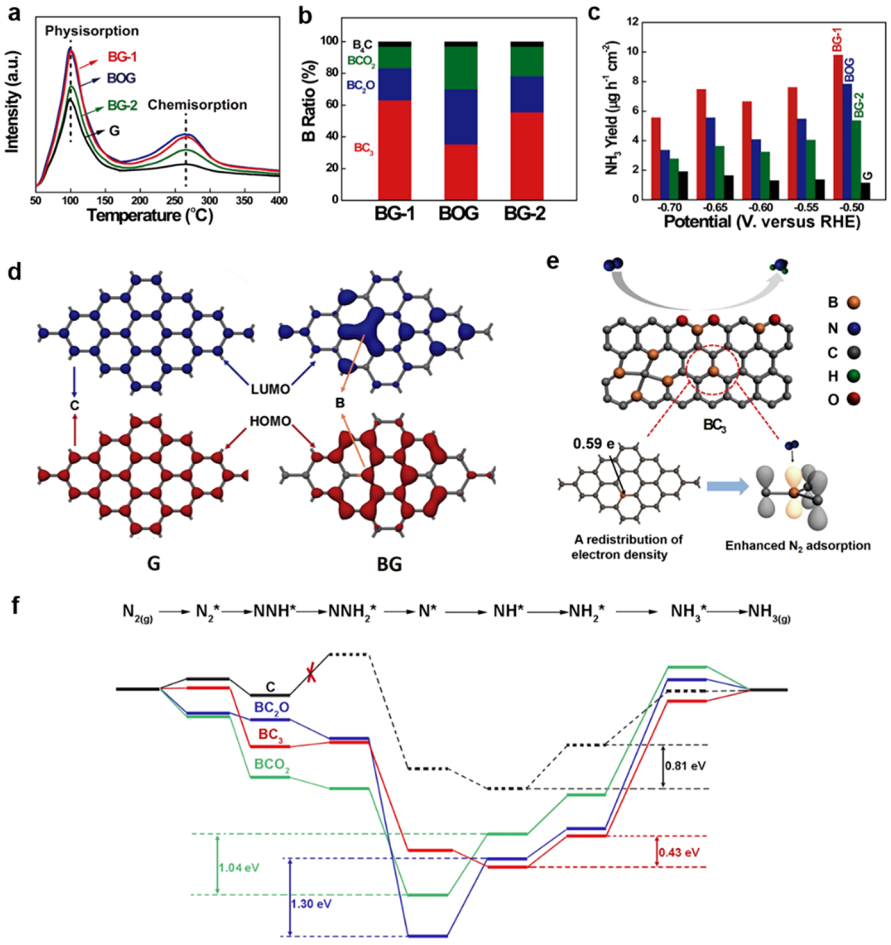

Figure 3. N_2 TPD curves (a), contents of various B types (b), and NH_3 formation rates (c) of BG and G samples. (d) Electron density of BG. (e) Schematic illustration of BG for electrochemical NRR. (f) Free-energy diagrams of BG and G samples for electrochemical NRR [Reproduced with permission from Figures 3−5 in ref 78. Copyright 2018 Elsevier].

of Lewis acid H^+, thus suppressing HER.[74−77] Along this line, a series of B-doped graphenes (BGs) were obtained by a carbonization of H_3BO_3 and graphene oxide.[78] Temperature-programmed desorption (TPD) demonstrated that chemisorption of N_2 molecules on BG samples is obviously enhanced and shows dependence on the B content (Figure 3a). Consequently, when used for electrochemical NRR, the activity of BG depends on the boron content and structures (B_4C, BC_3, BC_2O, and BCO_2) (Figure 3b). The catalyst with a doping level of 6.2 atom % and a high percentage of BC_3 provides an NH_3 formation rate of 9.8 $\mu g\ h^{-1}\ cm^{-2}$ and an FE of 10.8% at −0.5 V, 5 and 10 times higher than that of pristine graphene, respectively (Figure 3c). To demonstrate the NRR trend of catalysts with different boron content and structures, the molecular orbitals were modeled by DFT calculations. As shown in Figure 3d, after B doping, the electron densities of both HOMO (red) and LUMO (blue) are obviously redistributed resulting in the breaking of intrinsic equilibrium. The positive charge of B dopant (+0.59 lel) provides enhanced binding capability to N_2, thus serving as catalytic sites for electrochemical N_2 conversion to NH_3 (Figure 3e). Therefore, the increased B doping level enhances the electrocatalytic NRR performance. Among different B−C structures, the G-like BC_3 structure enables the lowest energy barrier (0.43 eV) for the potential-determining step of NH_2* formation, serving as major active centers for NRR (Figure 3f).

Chalcogen/Oxygen Group Element Doping. In addition to familiar N- and B-doping, chalcogen/oxygen group elements (e.g., O, S, Se, and Te) were also used as dopants to synthesize electrocatalysts with tunable NRR activities. O-doped graphene made by Ar annealing of sodium gluconate represented an efficient catalyst for NRR.[79] Experimental results revealed that O-doped graphene showed a relatively high FE of 12.6% and large NH_3 formation yield of 21.3 $\mu g\ h^{-1}\ mg_{cat}^{-1}$ in 0.1 M HCl. A mechanism exploration by DFT calculation suggested that the oxygen containing groups can facilitate NRR and the C═O and O−C═O groups decrease energy barriers for the potential-determining step more effectively compared to the C−O group. The same group also reported that the chemically oxidized carbon nanotube (O−CNT) is an NRR catalyst in neutral $LiClO_4$ solution. O−CNT displays a similar FE (12.5%) with O−G and a relatively large NH_3 formation yield of 32.33 $\mu g\ h^{-1}\ mg_{cat}^{-1}$.[80] Different from O-doped graphene, C−O groups in O−CNT show a stronger N_2 absorption energy than that of C═O, OH, and COOH groups, which play key role for catalytic NRR. In addition, research found S doping also strengthened NRR performance of graphene.[81,82] The resulting S-doped graphene showed a high selectivity for NRR in acid conditions and a remarkable durability with no FE and NH_3 yield decay after multiple recycle measurements. Theoretical calculations shown that the electrocatalytic activity was induced by the electron

https://doi.org/10.1021/acssuschemeng.1c00575
ACS Sustainable Chem. Eng. 2021, 9, 7687−7703

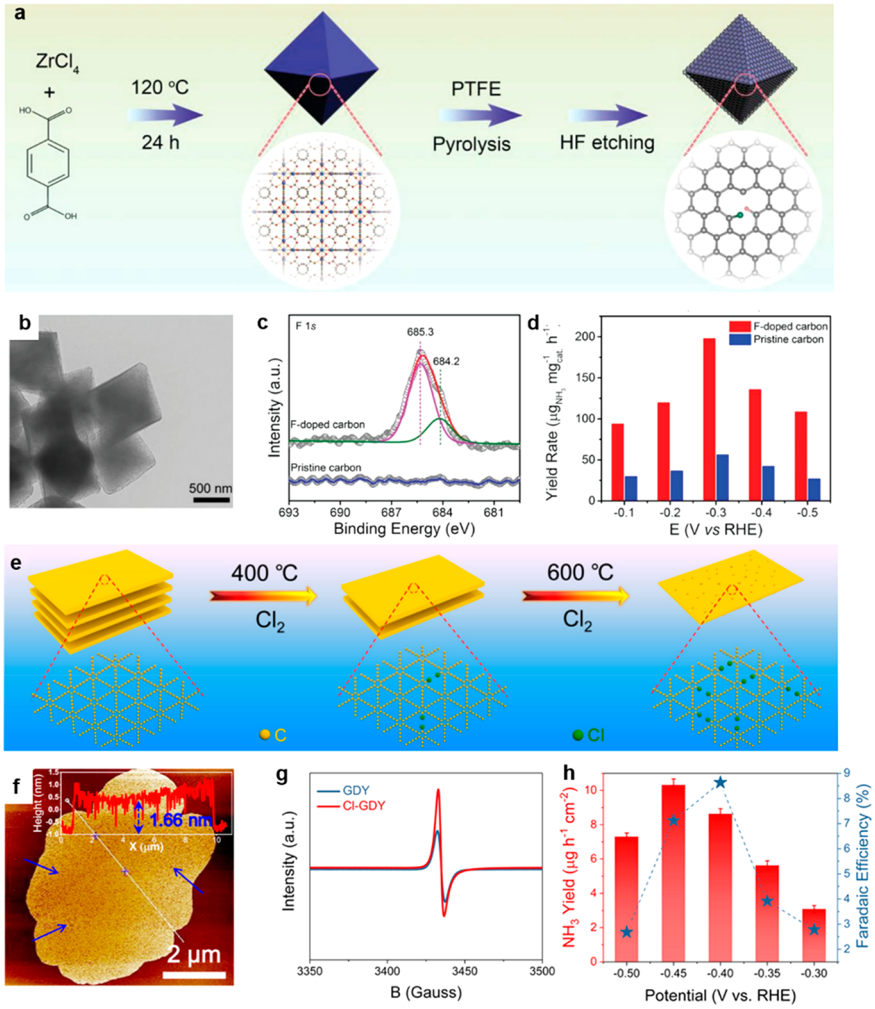

Figure 4. (a) Schematic synthesis process of F-doped carbon. (b) TEM image of F-doped carbon. F 1s XPS spectra (c) and NH_3 yield rate (d) for F-doped carbon and pristine carbon with F-doped carbon as a catalyst [Reproduced with permission from Figures 1−3 in ref 85 (a−d). Copyright 2020 Wiley-VCH]. (e) Scheme of the synthesis process for Cl-GDY. (f) AFM image of Cl-GDY. (g) EPR spectra of GDY and Cl-GDY. (h) NH_3 formation rates and FE of Cl-GDY [Reproduced with permission from Figures 1−4 in ref 87 (e−h). Copyright 2019 American Chemical Society].

density redistribution of carbon atoms near the substituted S atoms. Notably, similar to N and B atoms, S atoms in carbon nanospheres improve both the capability for chemisorption and physisorption of N_2.[83] Recently, with a MOF-derived nanoporous carbon as platform, Qiao et al. systematically evaluated the performance of chalcogen/oxygen group element (O, S, Se, and Te) doped carbons for NRR by theoretical calculations and experimental research.[84] DFT calculation proposed that the carbon neighboring the dopant is the active center for electrocatalytic NRR. Charge-rich carbon atoms induced by adjacent elements S (2.5), Se (2.4), and Te (2.1) with low electronegativity favor N_2 adsorption, while pristine and electron-deficient carbons with O (3.5) doping are unfavorable for N_2 adsorption with ΔE = 0 eV. Also, the formation of *NNH by the potential-determining step is facilitated by spin polarization. So, theoretical calculations predict that doping of heteroatom induced charge accumulation promotes the adsorption of N_2 on active C atoms, and spin polarization facilitates the potential-determining step of the formation of *NNH. Thus, Se- and Te-doped carbons with concentrated charge and polarized spin moments on the active sites were predicted to be more promising catalysts for NRR. Experiments confirmed that Te- and Se-doped catalysts have larger FEs of 4.67% and 3.92% than that of O- and S-doped catalysts (1.16% and 1.48%, respectively). In addition, Te- and Se-doped catalysts result in higher NH_3 formation rates and TOFs.

F-Doping. Similar to N, F possesses a higher electronegativity of 3.98 than that of C (2.55) and is thus a good dopant to introduce a Lewis acid site to carbon-based catalysts suppressing the undesirable HER. Along this line, a 3D F-doped porous carbon was developed for NRR by pyrolyzing UiO-66 in the presence of poly(tetrafluoroethylene) and following etching treatment by HF to remove ZrO_2 nanocrystals (Figure 4a and b).[85] Compared to pristine carbon, two peaks centered at 684.2 and 685.3 eV appeared in the F 1s XPS spectrum for F-doped carbon (0.55 at % F), which were attributed to the ionic C−F and semi-ionic C−F (Figure 4c). Electrochemical testing revealed that the highest FE reaches 54.8% for F-doped carbon in 0.05 M H_2SO_4 electrolyte which is 3 times higher than that of pristine carbon in the same conditions. More interestingly, the NH_3 formation rate is as high as 197.7 $\mu g\ mg_{cat}^{-1}\ h^{-1}$, a record value for metal-free catalyst under the same conditions (Figure 4d). As predicted, mechanistic study revealed that the electrochemical activity for NRR is improved due to the enhanced binding between N_2

https://doi.org/10.1021/acssuschemeng.1c00575
ACS Sustainable Chem. Eng. 2021, 9, 7687−7703

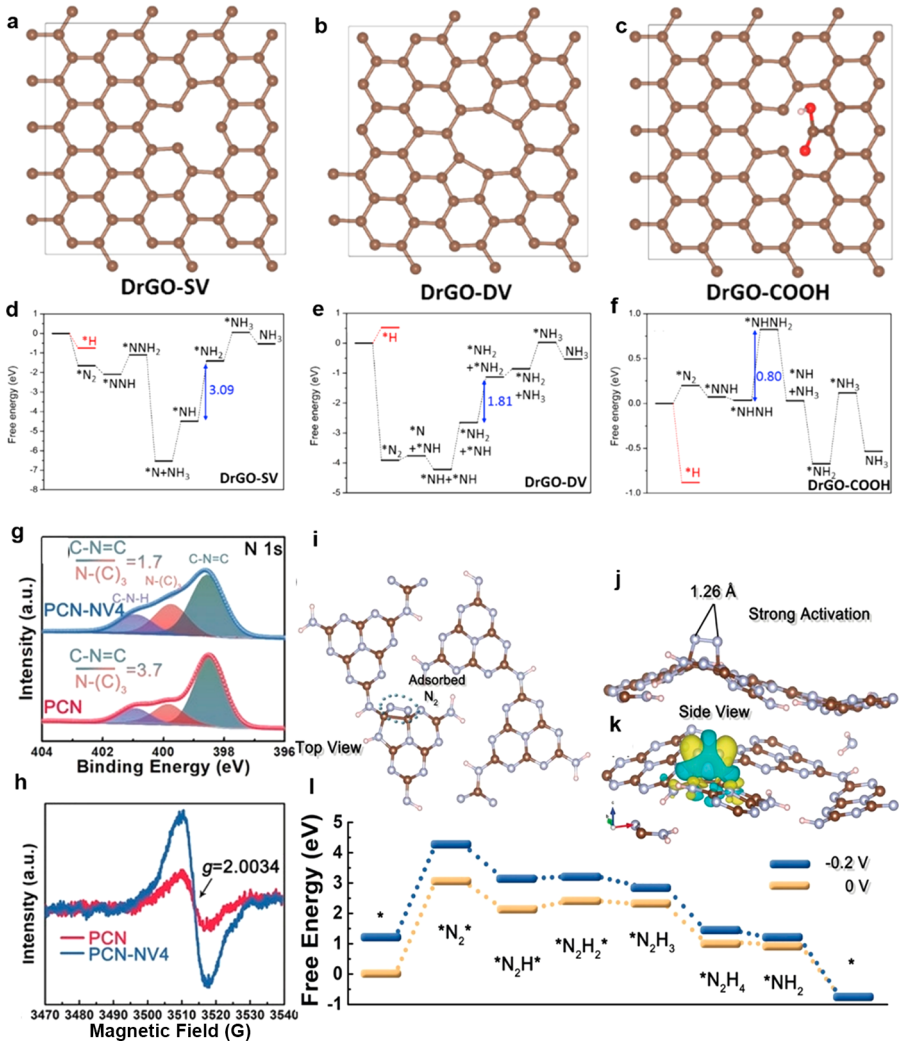

Figure 5. (a–c) Atomic configurations with various defect structures for theoretical calculations. (d–f) Free energy diagrams of NRR on various defect sites [Reproduced with permission from Figure 1 in ref 101 (a–f). Copyright 2019 Elsevier]. N 1s XPS (g) and EPR (h) spectra for PCN and PCN-NV_4. (i) N_2 adsorption configuration on nitrogen vacancy of PCN. (j and k) Charge density variation of the vacancy-rich PCN with N_2 adsorption; the blue and yellow iso-surfaces stand for charge depletion and accumulation, respectively. (l) Gibbs free energy of electrochemical NRR on N vacancy engineered PCN [Reproduced with permission from Figures 1 and 2 in ref 103 (g–i). Copyright 2018 Wiley-VCH].

and the Lewis acid C site created by F-doping, which facilitates the dissociation of N_2 to $*N_2H$. A similar mechanism has also been demonstrated on F-doped graphene toward N_2 electroreduction.[86]

Cl-Doping. As a lamellar carbon allotrope, graphdiyne with a tunable electronic structure and superior electrical conductivity enable it a possible candidate to catalyze N_2 conversion to NH_3. Duan et al. reported a Cl-doped ultrathin graphdiyne (Cl-GDY) for NRR by a simple Cl_2 corrosion process. The corrosion strategy introduced a Cl dopant but also etched host graphdiyne into ultrathin layer materials (Figure 4e).[87] The thickness of as-prepared Cl-GDY is around 1.66 nm (Figure 4f), and C, Cl, and O elements are homogeneously dispersed throughout the Cl-doped material. The doping degree of Cl is about 6.49 at %. The electron paramagnetic resonance (EPR) spectrum of Cl-GDY shows an obvious signal at g = 2.003 indicating that the Cl doping redistributes the extra electrons to neighboring C by the delocalized π-conjugated networks and results in a potential activation on N_2 (Figure 4g). Electrochemical measurement was conducted in 0.1 M HCl with N_2 saturation and the FE and NH_3 formation rate were determined to be 8.7% and 10.7 $\mu g\ h^{-1}\ cm^{-2}$, respectively (Figure 4h). The control experiments and isotopic labeling experiment with $^{15}N_2$ as feeding gas showed that NH_3 is indeed from NRR rather than contamination. DFT calculation showed energy barrier of the potential-limiting step (the largest energy barrier step) of HNN* formation is reduced by 0.11 eV after Cl-doping, implying Cl-GYD is more favorable for NRR than pristine structure of GYD.

P-Doping. P-doping was independently explored for NRR electrocatalysis by two different groups.[61,62] Hu et al. revealed that P-doped carbon nanotubes (P-CNTs) show an impressive catalytic performance for NRR with a partial current density for NH_3 production of 0.61 mA cm^{-2} at −1.1 V resulting in a NH_3 formation rate of 24.2 $\mu g\ h^{-1}\ mg_{cat}^{-1}$.[61] The superior activity was resulted from the electron-deficient phosphorus sites with Lewis acidity as revealed by experimental and theoretical investigations. Similarly, Sun et al. found that P-doped graphene (PG) can facilitate NRR efficiently with a remarkable NH_3 formation of 32.33 $\mu g\ h^{-1}\ mg_{cat}^{-1}$ and a FE of 20.82% at −0.65 V in 0.5 M $LiClO_4$.[62] Theoretical calculation

https://doi.org/10.1021/acssuschemeng.1c00575
ACS Sustainable Chem. Eng. 2021, 9, 7687−7703

shows that P-atom features a high electron state around a Fermi energy of PG resulting in a higher ability to interact with surface adsorbed molecules, e.g., N_2.

3.2. Co-Doping. The doping strategy for performance enhancement involves the electron and spin density redistribution and the resulting electron-deficient or -rich active sites.[59] Co-doping with two different heteroatoms, such as N/B, N/S, and N/P, can induce new nonelectron neutral sites by the synergistic effects between the dopants and thus increase the ORR, CO_2RR, and OER performance.[59,88−91] Inspired by these, Wang et al. constructed a metal-free NRR carbon catalyst by pyrolysis of organic precursor.[92] The doping content and bond states were controlled by tuning experimental conditions. Both theoretical calculations and practical experiments suggested that the substitutions of B−N pairs into basal plane of graphitic sheets would act active triggers and the edge carbon atoms near to B−N pairs are the catalytic centers toward the NRR. Meanwhile, the N/B codoping significantly suppressed the HER activity, confirmed by the high adsorption free-energy for *H species (0.65 eV). As a result, an NH_3 production rate of 7.75 μg h^{-1} mg^{-1} together with an excellent FE of 13.79% was achieved on this carbon catalyst. Besides, the B/N codoped porous carbon nanofiber (B/N-CNF) was developed and evaluated for NRR in an alkaline electrolyte by Hou et al.[93] The highest FE of B/N-CNF is 13.2%, 15 times more than that of the N-CNF (0.9%) and 3.8 times more than B-CNF under the same conditions. N-Doping could enhance electron conductivity, while B atoms facilitate N_2 adsorption and subsequent electron transfer to yield NH_3. An independent work was reported by Yang et al. with B/N-codoped carbon nanospheres as the NRR catalyst in acidic solution.[94] BC_3 and B−N species were confirmed to be the active centers, resulting in lower energy barrier for electrochemical N_2 to NH_3 conversion. BNC-NS showed a higher FE (8.1%) and NH_3 formation rate (15.7 mg h^{-1} mg_{cat}^{-1}) than those of N-doped NS (5.5% and 8.4 mg h^{-1} mg_{cat}^{-1}, respectively).

4. INTRINSIC DEFECTIVE CARBONS

Edge sites and topological defects are intrinsic in carbon materials and can endow the carbon matrix with different electronic structures and functionalities. Edge sites mainly contain vacancies at the edges and dangling groups. Topological defects include inherent topologic vacancies and deformations at both edges and carbon matrix and are usually formed naturally because of crystalline disorder or during the synthesis process.[95] It has been confirmed that the charge density of C close to these defects are significantly different from that of the basal-plane C, showing efficient electrocatalytic activities for a couple of electrochemical applications.[96−100] Therefore, creating effective edge sites and topological defects in a carbon matrix is also an alternative pathway to endow carbons with highly active sites.

Recently, a reduced graphene oxide with tunable defects (DrGO) was reported as NRR electrocatalyst under mild conditions by Sun et al.[101] To identify the effective active sites for NRR, DFT calculations were performed on various defect structures including oxygen-containing functional groups, structural defects in the basal plane, and on edge sites. They discovered that the defect structures with unsaturated carbon (single vacancy (SV), double vacancy (DV), and −COOH) (Figure 5a−c) could only activate N_2. As such, the free energy of N_2 binding ($\Delta G(*N_2)$) and H_2 binding ($\Delta G(*H)$) on different defective carbons were calculated. For DrGO-DV, the $\Delta G(*N_2)$ (−3.91 eV) was greatly more negative than $\Delta G(*H)$ (0.52 eV), implying a high $*N_2/*H$ selectivity (Figure 5d). Similarly, the $\Delta G(*N_2)$ of DrGO-SV (−1.65 eV) was also much more negative than $\Delta G(*H)$ (−0.75 eV) (Figure 5e). Compared to these two defects, DrGO-COOH showed a lower $*N_2/*H$ selectivity (Figure 5f). To confirm the calculations, a series of DrGO samples were synthesized by a hydrothermal reaction at different temperatures. The degree of vacancy defect increased with increased temperature, as revealed by the characteristic peak of sp^3 C−C. The samples containing defects display a much lower overpotential of 0.126 V than N-doped porous carbon (0.38 V). NH_3 yield reached to 7.8 $\mu g{\cdot}h^{-1}$ mg^{-1} with an FE of 22% in acid conditions and 7.4 μg h^{-1} mg^{-1} with an FE of 10.8% in alkaline conditions.

Moreover, the vacancy defects, used in combination with other strategies such as heteroatom doping, could further boost the electrocatalytic NRR due to the specific adsorption configuration and charge exchange of heteroatom and carbon vacancies with reactant.[100,102] For example, Mukherjee et al. demonstrated that an N_2 molecule could be favorably attracted by one carbon vacancy assisted by the pyridinic N_3 moiety, and the N≡N bond length of the adsorbed N_2 was elongated from 1.10 to 1.37 Å thus favoring the breakage of the strong N−N bond. The optimized samples exhibited a remarkable NH_3 production rate (3.4×10^{-6} mol cm^{-2} h^{-1}) with an FE of 10.2% at −0.3 V using aqueous 0.1 M KOH electrolyte, far exceeding the performance of pristine N-doped carbon.[69]

A defect engineering strategy was also adopted to synthesize a series of two-dimensional (2D) sheetlike polymeric carbon nitride (PCN) with tunable nitrogen vacancies (NVs) by the recalcination treatment in Ar atmosphere.[103] PCN with NVs showed a lower ratio of C−N═C/N−$(C)_3$ of 1.7 than that of pristine PCN (3.7), suggesting that the NV is preferentially located at a N_2C (two-coordinated N) site (Figure 5g). Furthermore, the introduction of NVs could redistribute the extra electrons to neighboring Cs by the delocalized π-conjugated networks of PCN, indicated by an enhanced signal at g = 2.0034 in EPR (Figure 5h). DFT calculations revealed that electrons on neighboring C are transferred to the adsorbed N_2 and N≡N bond strength is increased to 1.26 Å from the initial 1.0975 Å manifesting the N_2 activation (Figure 5i−k). An alternating hydrogenation mechanism considers the free energy of the pathways with the lowest energy (Figure 5l). As a result, PCN with abundant NVs gives the highest FE (11.59%) and NH_3 formation yield (8.09 μg h^{-1} mg_{cat}^{-1}), 10 times more compared to pristine PCN. Subsequently, Liu et al. reported N-defective carbon nitride supported on carbon paper (CN/C) as NRR electrocatalysts with a peak NH_3 production rate of more than 2.9 μg mg_{cat}^{-1} h^{-1} (−0.3 V) and an FE of 62.1%. The impressive NRR activity of the CN/C catalyst is induced by abundant C═N−C N_2C vacancies, fast electron transport among CN layers, and efficient charge transfer at the CN/C interfaces.[104]

5. ATOMIC METAL SPECIES COORDINATED CARBONS

In nature, NRR progresses easily at nitrogenases with FeMo or FeV cofactor.[4] Inspired by this, structures mimicking nitrogenases with Mo or Fe site coordinated by various of ligands were synthesized and confirmed to be active for NRR.[4,7,105−108] Those homogeneous catalysts feature well-defined structures comprising center metal and ligands with

https://doi.org/10.1021/acssuschemeng.1c00575
ACS Sustainable Chem. Eng. 2021, 9, 7687−7703

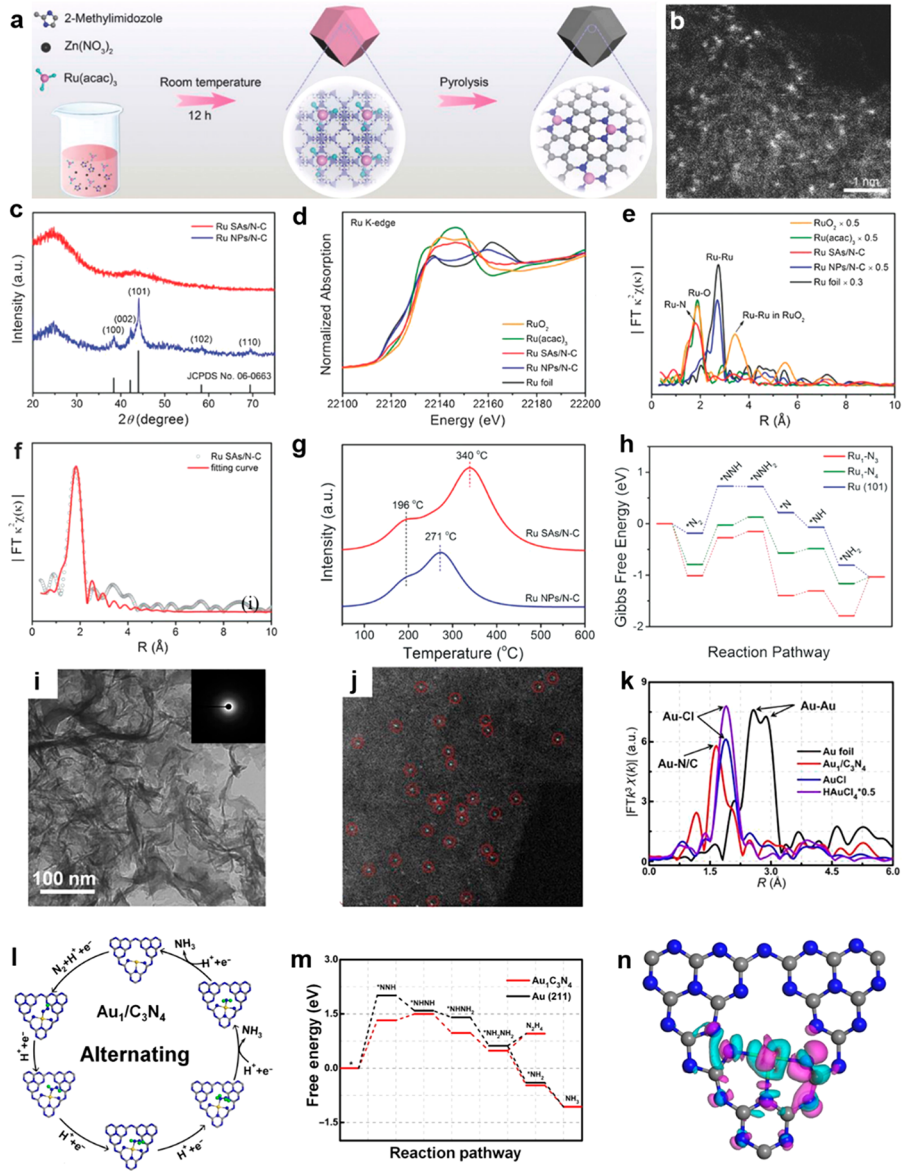

Figure 6. (a) Synthetic process and (b) HAADF-STEM of Ru SAs/N−C. (c) XRD patterns of Ru NPs/N−C and Ru SAs/N−C. Ru K-edge XANES (d) and EXAFS (e) spectra of Ru SAs/N−C and a series of control samples. (f) EXAFS fitting result of Ru SAs/N−C. (g) N_2-TPD curves for Ru NPs/N−C Ru and SAs/N−C. (h) Free-energy diagrams of the NRR process on various sites [Reproduced with permission from Figures 1, 2, and 4 in ref 131 (a−h). Copyright 2018 Wiley-VCH]. TEM image (i), magnified HAADF-STEM image (j), and EXAFS spectra (k) of Au1/C_3N_4. (l) Atomic configurations at various states of NRR on Au_1/C_3N_4. (m) Free-energy profiles of NRR on different samples at zero potential. (n) Electron density variation of Au_1/C_3N_4 induced by Au single atoms dopant. Pink and cyan stand for electron depletion and accumulation, respectively. [Reproduced with permission from Figures 2, 3, and 5 in ref 133 (i−n). Copyright 2018 Elsevier].

coordinating sites and are easily accessible for mechanism exploration at the molecular level by several spectroscopic approaches and theoretical calculations.[4] However, homogeneous catalysts usually suffer from poor durability compared to heterogeneous catalysts.[109]

Recently, single-atom catalysts (SACs) have received great attention and emerged as attractive candidates in heterogeneous catalysis.[110,111] For highly active carbon-based SACs, single metal atoms are coordinated to these N, S, and O dopants creating similar active sites as those on the metal−*N*-macrocycles on carbon support. The charge density of the isolated metal site is tunable because of the various metal atoms and dopants, enabling them as suitable for various catalytic reactions.[110,112,113] In comparison with traditional heterogeneous catalyst, carbon-based SACs have evenly dispersed active sites similar with homogeneous catalysts, enabling them simultaneous advantages of both heterogeneous and homogeneous catalysts.[114−116] These inspired the study on integration of the "ligand−metal" concept from homogeneous molecular catalysis with carbon-based SACs for NRR in heterogeneous electrocatalysis.[111,117−119]

5.1. Theoretical Calculation on Carbon-Based SACs for NRR. Several theoretical calculations were carried out, trying to predict the feasibility of SACs for NH_3 formation by electrochemical NRR.[34,120−128] An example is the DFT calculation carried out by Wang et al. with Ru atoms supported on a series of carbon materials.[129] The active centers were the single Ru atom coordinated with N or C atoms in the carbon matrix. N_2 adsorption on the surface of these SACs is crucial for the subsequent NRR, and thus, the

https://doi.org/10.1021/acssuschemeng.1c00575
ACS Sustainable Chem. Eng. 2021, 9, 7687−7703

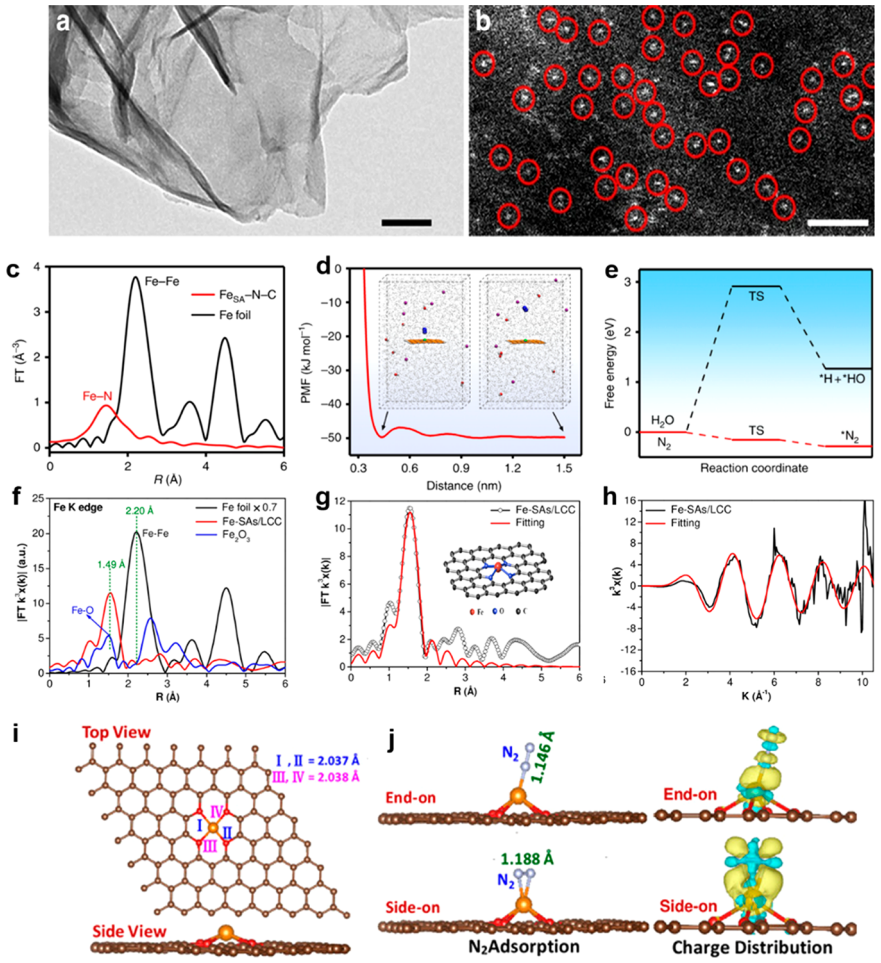

Figure 7. TEM (a) and HAADF-STEM (b) images of FeSA–N–C. (c) Fe K-edge XANES for samples. PMF of N_2 adsorption (d) and free energy diagrams for the NRR (e) of FeSA–N–C. [Reproduced with permission from Figures 1 and 4 in ref 146 (a–e). Copyright 2019 Nature]. (f) EXAFS spectra for Fe-SAs/LCC and other samples. EXAFS (g) and corresponding Fe K-edge EXAFS (h) fitting curves for Fe-SAs/LCC. (i) Optimized Fe–$(O–C_2)_4$ framework. (j) Configurations with N_2 adsorption on isolated Fe site and Bader charge distribution for $*N_2$. [Reproduced with permission from Figures 2 and 3 in ref 148 (f–j). Copyright 2020 Wiley-VCH].

free energies of adsorption with N_2 coordination in vertical and parallel framework were subsequently calculated. The N_2 molecule with vertical configuration were preferable, considering their high adsorption energy. Further exploration of the reaction mechanism displayed that associate mechanism featuring lower energy barrier is more favorable for the formation of NH_3 on the three catalysts. Although the onset potentials are similar, the potential-limiting step varies with supports, implying an effect of supports on electrochemical NRR. Similarly, Qiao et al. explored a series of N-doped carbons (NCs) as platform offering various coordination environments for 20 transition metal, leading to 60 SACs.[125] Then, an overview of the potential of TM–SACs as NRR electrocatalyst were built up by DFT calculations. The results revealed the inherent performance of these SACs is related to the adsorption energy (ΔE_{N*}) of N adatom. Furthermore, they found that the difference of ΔE_{N*} originates from the effect of metal sites on the bonding/antibonding orbital populations. Besides, the variety of supports also influences the catalytic activity by offering different ligand environments, which is similar to the operation of homogeneous catalysts. This study shows that the matching of the support and metal active center to reduce the potential of key intermediate formation is an effective way to design NRR electrocatalysts.

5.2. Noble- and Rare-Metal Based SACs. Inspired by theoretical research, experiments reported various SACs.[130] For example, the Ru-based SACs with isolated Ru atom embedded on N-doped carbon (Ru SAs/N–C) were synthesized through pyrolyzing the Ru-containing derivative of ZIF-8 (Figure 6a).[131] For Ru SAs/N–C, the individual Ru atom was uniformly dispersed on the carbon support (Figure 6b), and no obvious Ru nanoparticle was found (Figure 6c). The Ru atoms with a valence of +3 were coordinated with N atoms, forming Ru–N bonds and no obvious Ru–Ru bond was detected (Figure 6d–f). The mass loading of the Ru atom was around 0.18% determined by inductively coupled plasma atomic emission spectroscopy (ICP-AES). An impressive FE of 29.6% was obtained at −0.2 V, and the corresponding NH_3 formation rate reached 120.9 $\mu g\ mg_{cat}^{-1}\ h^{-1}$, higher than most of reported values. N_2-TPD demonstrated that both pyrolyzed ZIF-8 and Ru species show strong bonding of N_2, thus facilitating the adsorption of N_2 (Figure 6g). DFT calculations further revealed that the energy barrier for N_2 dissociation on the surface of $Ru_1–N_3$ (0.73 eV) and $Ru_1–N_4$ (0.77 eV) are lower than that (0.91 eV) on Ru (101), thereby enabling an impressive activity of Ru SAs/N–C (Figure 6h). Similarly, Ru@ZrO_2/NC were prepared by pyrolyzing UiO-66-NH_2.[130] The uncoordinated $-NH_2$ groups in UiO-66-NH_2 could

https://doi.org/10.1021/acssuschemeng.1c00575
ACS Sustainable Chem. Eng. 2021, 9, 7687–7703

stabilize the $RuCl_3$ and further block the Ru assembling during the pyrolysis process. As a result, 88% of Ru are single atoms dispersed on NC, of which the size falls in the range of 0.1−0.2 nm. The loading content of Ru was determined to be 0.1 wt %. In contrast to Ru nanoparticles, a stable NH_3 production rate of 3.665 mg h^{-1} mg_{Ru}^{-1} was obtained at −0.21 V by single Ru atoms dispersed on NC. DFT calculations suggested that Ru sites with oxygen vacancies are possibly the major active centers, which can improve N_2 adsorption, stabilize intermediate *NNH, and destabilize *H. The O vacancy in ZrO_2 facilitates the catalytic performance of individual Ru sites for the formation of NH_3 and suppresses the competitive HER but does not act as an active center. Besides, Ru SAs/g-C_3N_4[132] also shows high activity for electrochemical NRR under mild conditions.

Au single atoms supported on N-doped porous carbon (Au SAs-NDPCs) were investigated by a classic impregnation method with $HAuCl_4$ as precursor.[134] The Au single atom was evenly dispersed on a porous carbon matrix by forming Au−N bonds. The mass percentage of Au in AuSAs-NDPCs was 0.205 wt %. The highest FE was 12.3%, and the corresponding NH_3 formation yield was 2.32 $\mu g\ h^{-1}\ cm^{-2}$. Wu et al. explored atomically dispersed Au_1 supported on carbon nitride (Au_1/C_3N_4) for electrochemical NRR in H_2SO_4 electrolyte (Figure 6i and j).[133] Atomic Au was confirmed by the absence of an Au−Au bond and the peak of 1.65 Å assigned to Au−N in near edge X-ray absorption fine structure (NEXAFS) (Figure 6k). The valence of Au in Au_1/C_3N_4 is +1 determined by XANES and XPS analysis. Compared to C_3N_4 and Au NPs/C_3N_4 (Au nanoparticles loaded on C_3N_4), Au_1/C_3N_4 showed higher FE, up to 11% with an NH_4^+ formation rate of 1305 $\mu g\ h^{-1}\ mg_{Au}^{-1}$. DFT calculations shown that ΔG for the reduction of N_2 to *NNH (rate determining step) on Au_1/C_3N_4 (1.33 eV) is smaller than that (2.01 eV) on Au (211), meaning that the isolated Au atom in Au/C_3N_4 induces the high activity of NRR (Figure 6l and m). Furthermore, the Bader charge population analysis revealed that a positive charge (0.56 |e|) on Au was induced by the charge transfer from the Au to the g-C_3N_4 (Figure 6n). The electron depletion of Au atom may shift its d-orbital position toward the Fermi level, thus enhancing its adsorption with intermediates and subsequently leading to a high activity of NRR.

As the metal component in nitrogenase,[135] Mo-based NRR SACs were studied extensively.[120,121] Xin et al. selected a 3D N-doped porous carbon as the support for embedding of single atom Mo (SA-Mo/NPC).[136] The Mo loading in SA-Mo/NPC is 9.54 wt %. EXAFS confirmed that most of the Mo atoms are isolated from each other and bonded with C or N in SA-Mo/NPC, and a small fraction of the Mo atom is in the form of clusters, weakly interacting with neighboring Mo atoms. The FE and NH_3 yield rate were 14.6 ± 1.6% and 34.0 ± 3.6 $\mu g\ mg_{cat}^{-1}\ h^{-1}$ in 0.1 M KOH. The impressive catalytic activity was resulted from the high density and uniform dispersion of active sites and hierarchically porous carbon frameworks.

5.3. Earth-Abundant Transition Metal-Based SACs. The 3d transition metals (e.g., Fe, Co, Ni and Cu) have been extensively investigated for electrochemical applications.[137−145] Recently, these earth abundant metals were also studied for electrochemical NRR. An isolated Fe-based single site catalyst embedded on N-doped carbon (ISAS-Fe/NC) was obtained by carbonization of Fe-ZIF method.[147] The Fe content was determined as 4.2 wt %. EXAFS of ISAS-Fe/NC shows one main peak at 1.5 Å assigned to the Fe−N, consistent with the wavelet transform (WT) plots where only Fe−N signal of WT maximum at 3.7 $Å^{-1}$ was detected. The FE reached as high as 18.6 ± 0.8% with a NH_3 production rate of 62.9 ± 2.7 $\mu g\ h^{-1}\ mg_{cat}^{-1}$. DFT calculations suggested that Fe single atom in Fe−N_4 configuration favors N_2 adsorption and subsequent activation, suggesting high electrochemical NRR activity and selectivity. Yan et al. prepared Fe single atoms embedded in N-doped carbon framework (FeSA-N−C) by the calcination of a polypyrrole-iron complex for efficient electrochemical N_2 conversion to NH_3.[146] FeSA-N−C showed the 2D graphene-like morphology and possessed atomically isolated Fe atoms (Figure 7a−c). The onset potential of FeSA-N−C for NRR was around 0.193 V, showing 200 mV positive shift compared to that of N-doped carbon. More interestingly, the FE of FeSA-N−C reached 56.55% at a relative positive of 0 V, six times higher than that of Fe free sample. Both FE and onset potential are outstanding among the reported catalysts. Molecular dynamics simulations revealed that the FeSA-N−C structure could facilitate N_2 adsorption with a small energy barrier (2.38 kJ mol^{-1}, Figure 7d). The obtained high local N_2 concentration was favorable for the following adsorption with a particularly low ΔG of −0.28 eV. Strikingly, H_2O dissociation to *H was sluggish on FeSA-N−C with an energy barrier of 2.91 eV (Figure 7e). Similar to the above two studies, Fe/N-doped carbon nanotube (Fe-N/C) was synthesized with isolated Fe atoms by Zheng et al.[147] The highest NH_3 yield rate of 34.83 $\mu g\ h^{-1}\ mg_{cat}^{-1}$ was achieved with a FE of 9.28% at −0.2 V for Fe-N/C, while the efficiency was relatively low for N-doped carbon nanotube. Further exploration revealed that the NH_3 formation efficiency depends on pyridinic N rather than Fe. Both experimental and theoretical exploration revealed that Fe−N_3 configuration is responsible for NRR.

The SACs mentioned above are constituted by metal−nitrogen (M−N_x) configurations. Fe atoms embedded in the nitrogen-free carbon support with an Fe−$(O-C_2)_4$ coordination bond (Fe-SAs/LCC) were reported recently by Zhao et al.[148] For Fe-SAs/LCC, the isolated Fe atom was anchored on carbon matrix via the Fe−$(O-C_2)_4$ coordination, and no obvious Fe−Fe bond was observed (Figure 7f−h). DFT calculation identified Fe−$(O-C_2)_4$ as the active center (Figure 7i). The Bader charge analysis suggested that the electron transfer from Fe−$(O-C_2)_4$ sites to N_2 occurs through a back-donation mechanism, by which N_2 is activated (Figure 7j). Fe-SAs/LCC loaded on a carbon cloth electrode can afford an NH_3 formation rate of 32.1 $\mu g\ h^{-1}\ mg_{cat}^{-1}$ and an FE of 29.3% in 0.1 M KOH.

Based on the theoretical calculations by Qiao et al., Co features lowest onset potential in 3d metals, implying that Co is a promising candidate for electrochemical NRR.[125,149] Thus, a series of Co/N-doped carbon composite catalysts were synthesized by pyrolysis of Co-based ZIF-67.[150] The obvious Co nanoparticles along with single Co sites were observed on an N-doped carbon surface. The nitrogen and cobalt species could be tuned by simply changing the pyrolysis temperature from 400 to 700 °C. The highest activity was obtained with an FE of 10.1% at −0.1 V and an NH_3 formation rate of 5.1 $\mu g\ h^{-1}\ mg_{cat}^{-1}$ at −0.4 V. Single Co sites coordinated with pyrrolic N groups were assigned to be active centers for NRR. Besides, an atomically dispersed Ni catalyst was obtained by calcining a Ni- and Zn-based bimetallic metal organic framework (BMOF).[151] The XANES pattern revealed that the valence of Ni in Ni−N_x−C is between 0 and +2, and no Ni−C signal was detected. A dominant peak of 1.41 Å in Fourier-

https://doi.org/10.1021/acssuschemeng.1c00575
ACS Sustainable Chem. Eng. 2021, 9, 7687−7703

transformed EXAFS of Ni−N_x−C was assigned to Ni−N coordination, and the number of coordinated sites was estimated between 3 and 4. The highest FE of 21 ± 1.9% was obtained at −0.2 V, and the optimal NH_3 production rate of 115 $\mu g\ cm^{-2}\ h^{-1}$ was achieved at −0.3 V. DFT calculations confirmed that the Ni−N_3 sites are favorable for the high catalytic performance.

As a 3d transition metal, Cu was also explored for electrochemical NRR.[152,153] Cu SAs attached in a porous N-doped carbon framework (NC−Cu) were achieved by a surfactant-assisted synthesis strategy.[154] A dominant peak of 1.48 Å attributed to Cu−N/C coordination was observed in the FT-EXAFS spectrum of NC−Cu, and no signal for Cu−Cu or Cu−O was observed, indicating uniform dispersion of Cu single atoms in a carbon matrix. The NH_3 formation rate and FE of the Cu-based SACs were ∼49.3 $\mu g\ h^{-1}\ mg_{cat}^{-1}$ and 11.7% with 0.1 M HCl as electrolyte, ∼53.3 $\mu g\ h^{-1}\ mg_{cat}^{-1}$ and 13.8% with 0.1 M KOH. DFT calculations suggested that the Cu−N_2 sites are favorable for the high NRR performance, rather than the previous report of Cu−N_4/N_3C configurations.[122]

6. CONCLUSIONS AND OUTLOOK

This review provides a comprehensive overview on carbon-based catalysts for electrochemical N_2-to-NH_3 conversion. For the heteroatom-doped carbon materials, adjacent heteroatoms possessing strong or weak electronic affinity induce charge and spin density redistribution in a carbon framework, leading to nonelectron neutral sites. The nonelectron neutral carbon or heteroatom as a Lewis acid facilitates N_2 adsorption, a prestep for NRR, and suppresses HER, giving high conversion efficiency to NH_3. A Co-doping strategy can improve density of active sites and thus further enhance the catalytic activity. For carbon materials with edge sites and topological defects, the charge densities of carbon atoms near these defects are significantly different from that of the basal-plane carbon, exhibiting improved NRR activity. For carbon-based SACs, atomically dispersed metal centers can be coordinated with N or other heteroatoms in a carbon matrix (e.g., M−N and M−O) and the unsaturated coordination environment leads to abundant charge transfer from the active metal to the support, leading to electron-deficient metal and high affinity for N_2 adsorption and subsequent activation.

The research in this field has progressed a lot, while several issues and challenges remain to be solved before practical applications can be realized. First, the current mechanistic understanding mainly relies on theoretical calculations, but NRR in solution is significantly complicated. Therefore, spectroscopic technologies such as in situ FTIR and mass spectrometry for the detection of intermediates are highly desired for mechanistic studies. Second, like molecular catalysts, the catalytic performance of SACs can be affected by the ligand effect. However, introduction of a specific functional group to the support of SACs is still a challenge because of harsh synthesis conditions such as high temperature. Therefore, facile synthesis and modification strategies of SACs should be developed. Third, some catalysts showed high faradaic efficiency of more than 50%, while high selectivity was only achieved at low overpotentials with a slow NH_3 formation rate. The faradaic efficiency decreased with more negative applied potentials where HER becomes dominant.

The selectivity is regulated by the adsorption strength between metal sites and the reactant as well as key intermediates. The optimum adsorption strength may be achieved by finely tuning the coordination environment with the following design strategies. (i) Inspired by the structure of bionitrogenase such as FeMo and FeV for nitrogen fixation, a dual-atom catalyst with different metal−atom coordination with heteroatom may be developed. (ii) The strategy combining doping and metal single atoms is also a perspective direction, which facilitates electron localization and regulates the adsorption strength of substrate and intermediates. (ii) The construction of defects on the carbon matrix embedded SACs also should be explored, suppressing the competing HER and facilitating NRR. These studies on various coordination environments of central metals are limited so far. We believe that the advances in these directions will give high FE and NH_3 formation rate in the future, so that the energy-intensive and fossil fuel-dependent Haber−Bosch process can be substituted by electrochemical NH_3 synthesis.

AUTHOR INFORMATION

Corresponding Authors

Fengshou Yu − *Tianjin Key Laboratory of Chemical Process Safety, National-Local Joint Engineering Laboratory for Energy Conservation in Chemical Process Integration and Resources Utilization, School of Chemical Engineering and Technology, Hebei University of Technology, Tianjin 300130, P. R. China; State Key Laboratory of Fine Chemicals, Dalian University of Technology (DUT), Dalian 116024, Liaoning, P. R. China*; Email: yfsh@hebut.edu.cn

N. Raveendran Shiju − *Catalysis Engineering Group, Van't Hoff Institute for Molecular Sciences, University of Amsterdam, 1090GD Amsterdam, The Netherlands*; orcid.org/0000-0001-7943-5864; Email: n.r.shiju@uva.nl

Author

Lu-Hua Zhang − *Tianjin Key Laboratory of Chemical Process Safety, National-Local Joint Engineering Laboratory for Energy Conservation in Chemical Process Integration and Resources Utilization, School of Chemical Engineering and Technology, Hebei University of Technology, Tianjin 300130, P. R. China*

Complete contact information is available at: https://pubs.acs.org/10.1021/acssuschemeng.1c00575

Notes

The authors declare no competing financial interest.

Biographies

https://doi.org/10.1021/acssuschemeng.1c00575
ACS Sustainable Chem. Eng. 2021, 9, 7687−7703

Lu-Hua Zhang is an Associate Professor at Hebei University of Technology. She obtained her Ph.D. at Dalian University of Technology in 2017 under the guidance of Prof. An-Hui Lu. Then, she worked as a postdoctoral research fellow in Prof. Yumeng Shi's group at Shenzhen University and Dr. Raveendran Shiju's Catalysis Engineering group at the University of Amsterdam. Currently, her research interests mainly focus on synthesis of porous nanocarbons and design of novel carbon-based catalysts for electrochemical energy conversion.

Fengshou Yu received his Ph.D. under the guidance of Prof. Licheng Sun and Prof. Fei Li from Dalian University of Technology in 2017. From February 2017 to February 2019, he worked as a Postdoctoral Researcher at the University of Amsterdam with Prof. Joost N. H. Reek. Currently he is a tenure track Associate Professor at Hebei University of technology. The main research in his group considers small molecule activation including N_2, CO_2, O_2, and H_2O through electrochemical and photochemical approaches.

N. Raveendran Shiju is an Associate Professor at the University of Amsterdam. He obtained his Ph.D. in catalysis from the National Chemical Laboratory, Pune, India. After postdoctoral stays in the UK and USA, he joined the University of Amsterdam as a faculty member. His research focuses on the engineering of heterogeneous catalysts in industrially important reactions including CO_2 conversion, biomass conversion, and lower alkane activation to chemicals and fuels.

■ ACKNOWLEDGMENTS

This work was supported by the National Natural Science Foundation of China (No. 21905073 and 22008048), "Hundred Talents Project" of Hebei Province (No. E2019050015), and the State Key Laboratory of Fine Chemicals (KF 1909).

■ REFERENCES

(1) Erisman, J. W.; Sutton, M. A.; Galloway, J.; Klimont, Z.; Winiwarter, W. How a Century of Ammonia Synthesis Changed the World. *Nat. Geosci.* **2008**, *1* (10), 636−639.
(2) Smil, V. Detonator of the Population Explosion. *Nature* **1999**, *400* (6743), 415−415.
(3) Smith, C.; Hill, A. K.; Torrente-Murciano, L. Current and Future role of Haber-Bosch Ammonia in a Carbon-Free Energy Landscape. *Energy Environ. Sci.* **2020**, *13* (2), 331−344.
(4) van der Ham, C. J. M.; Koper, M. T. M.; Hetterscheid, D. G. H. Challenges in Reduction of Dinitrogen by Proton and Electron Transfer. *Chem. Soc. Rev.* **2014**, *43* (15), 5183−5191.
(5) Hu, L.; Xing, Z.; Feng, X. Understanding the Electrocatalytic Interface for Ambient Ammonia Synthesis. *ACS Energy Lett.* **2020**, *5* (2), 430−436.
(6) Nagaoka, K.; Eboshi, T.; Takeishi, Y.; Tasaki, R.; Honda, K.; Imamura, K.; Sato, K. Carbon-free H_2 Production from Ammonia Triggered at room Temperature with an Acidic RuO_2/γ-Al_2O_3 Catalyst. *Sci. Adv.* **2017**, *3* (4), 1602747.
(7) Foster, S. L.; Bakovic, S. I. P.; Duda, R. D.; Maheshwari, S.; Milton, R. D.; Minteer, S. D.; Janik, M. J.; Renner, J. N.; Greenlee, L. F. Catalysts for Nitrogen Reduction to Ammonia. *Nat. Catal.* **2018**, *1* (7), 490−500.
(8) Wang, L.; Xia, M.; Wang, H.; Huang, K.; Qian, C.; Maravelias, C. T.; Ozin, G. A. Greening Ammonia toward the Solar Ammonia Refinery. *Joule* **2018**, *2* (6), 1055−1074.
(9) Shi, R.; Zhang, X.; Waterhouse, G. I. N.; Zhao, Y.; Zhang, T. The Journey toward Low Temperature, Low Pressure Catalytic Nitrogen Fixation. *Adv. Energy Mater.* **2020**, *10* (19), 2000659.
(10) Zhang, L.-H.; Mathew, S.; Hessels, J.; Reek, N. H. J.; Yu, F. Homogeneous Catalysts Based on First-Row Transition Metals for Electrochemical Water Oxidation. *ChemSusChem* **2021**, *14* (1), 234−250.
(11) Wang, L.; Chen, W.; Zhang, D.; Du, Y.; Amal, R.; Qiao, S.; Wu, J.; Yin, Z. Surface Strategies for Catalytic CO_2 Reduction: from Two-Dimensional Materials to Nanoclusters to Single Atoms. *Chem. Soc. Rev.* **2019**, *48* (21), 5310−5349.
(12) Ding, X.; Zhang, L.; Wang, Y.; Liu, A.; Gao, Y. Design of Photoanode-Based Dye-Sensitized Photoelectrochemical Cells Assembling with Transition Metal Complexes for Visible Light-Induced Water Splitting. *Coord. Chem. Rev.* **2018**, *357* (15), 130−143.
(13) Shao, M.; Chang, Q.; Dodelet, J.-P.; Chenitz, R. Recent Advances in Electrocatalysts for Oxygen Reduction Reaction. *Chem. Rev.* **2016**, *116* (6), 3594−3657.
(14) Guo, W.; Zhang, K.; Liang, Z.; Zou, R.; Xu, Q. Electrochemical Nitrogen Fixation and Utilization: Theories, Advanced Catalyst Materials and System Design. *Chem. Soc. Rev.* **2019**, *48* (24), 5658−5716.
(15) Qing, G.; Ghazfar, R.; Jackowski, S. T.; Habibzadeh, F.; Ashtiani, M. M.; Chen, C.-P.; Smith, M. R.; Hamann, T. W. Recent Advances and Challenges of Electrocatalytic N_2 Reduction to Ammonia. *Chem. Rev.* **2020**, *120* (12), 5437−5516.
(16) Zhu, X.; Mou, S.; Peng, Q.; Liu, Q.; Luo, Y.; Chen, G.; Gao, S.; Sun, X. Aqueous Electrocatalytic N_2 Reduction for Ambient NH_3 Synthesis: Recent Advances in Catalyst Development and Performance Improvement. *J. Mater. Chem. A* **2020**, *8* (4), 1545−1556.
(17) Liu, H.; Wei, L.; Liu, F.; Pei, Z.; Shi, J.; Wang, Z.-J.; He, D.; Chen, Y. Homogeneous, Heterogeneous, and Biological Catalysts for Electrochemical N_2 Reduction toward NH_3 under Ambient Conditions. *ACS Catal.* **2019**, *9* (6), 5245−5267.
(18) Shi, L.; Yin, Y.; Wang, S.; Sun, H. Rational Catalyst Design for N_2 Reduction under Ambient Conditions: Strategies toward Enhanced Conversion Efficiency. *ACS Catal.* **2020**, *10* (12), 6870−6899.
(19) Tang, C.; Qiao, S.-Z. How to Explore Ambient Electrocatalytic Nitrogen Reduction Reliably and Insightfully. *Chem. Soc. Rev.* **2019**, *48* (12), 3166−3180.
(20) van Tamelen, E. E.; Boche, G.; Greeley, R. An Organic-Inorganic System for Reaction with Nitrogen of the Air and

https://doi.org/10.1021/acssuschemeng.1c00575
ACS Sustainable Chem. Eng. 2021, 9, 7687−7703

Operation of a Facile Nitrogen Fixation-Reduction Cycle. *J. Am. Chem. Soc.* **1968**, *90* (6), 1677−1678.
(21) Van Tamelen, E. E.; Seeley, D. A. Catalytic Fixation of Molecular Nitrogen by Electrolytic and Chemical Reduction. *J. Am. Chem. Soc.* **1969**, *91* (18), 5194−5194.
(22) Chatt, J.; Pearman, A. J.; Richards, R. L. The Reduction of Mono-Coordinated Molecular Nitrogen to Ammonia in a Protic Environment. *Nature* **1975**, *253* (5486), 39−40.
(23) Chen, A.; Xia, B. Y. Ambient Dinitrogen Electrocatalytic Reduction for Ammonia Synthesis. *J. Mater. Chem. A* **2019**, *7* (41), 23416−23431.
(24) Chen, X.; Guo, Y.; Du, X.; Zeng, Y.; Chu, J.; Gong, C.; Huang, J.; Fan, C.; Wang, X.; Xiong, J. Atomic Structure Modification for Electrochemical Nitrogen Reduction to Ammonia. *Adv. Energy Mater.* **2020**, *10* (3), 1903172.
(25) Zhai, Y.; Zhu, Z.; Zhu, C.; Chen, K.; Zhang, X.; Tang, J.; Chen, J. Single-Atom Catalysts Boost Nitrogen Electroreduction Reaction. *Mater. Today* **2020**, *38*, 99−113.
(26) Wang, Z.; Hu, X.; Liu, Z.; Zou, G.; Wang, G.; Zhang, K. Recent Developments in Polymeric Carbon Nitride-Derived Photocatalysts and Electrocatalysts for Nitrogen Fixation. *ACS Catal.* **2019**, *9* (11), 10260−10278.
(27) Kong, X.; Peng, H.-Q.; Bu, S.; Gao, Q.; Jiao, T.; Cheng, J.; Liu, B.; Hong, G.; Lee, C.-S.; Zhang, W. Defect Engineering of Nanostructured Electrocatalysts for Enhancing Nitrogen Reduction. *J. Mater. Chem. A* **2020**, *8* (16), 7457−7473.
(28) Wang, P.; Chang, F.; Gao, W.; Guo, J.; Wu, G.; He, T.; Chen, P. Breaking Scaling Relations to Achieve Low-Temperature Ammonia Synthesis Through LiH-Mediated Nitrogen Transfer and Hydrogenation. *Nat. Chem.* **2017**, *9* (1), 64−70.
(29) Montoya, J. H.; Tsai, C.; Vojvodic, A.; Nørskov, J. K. The Challenge of Electrochemical Ammonia Synthesis: A New Perspective on the Role of Nitrogen Scaling Relations. *ChemSusChem* **2015**, *8* (13), 2180−2186.
(30) Singh, A. R.; Rohr, B. A.; Schwalbe, J. A.; Cargnello, M.; Chan, K.; Jaramillo, T. F.; Chorkendorff, I.; Nørskov, J. K. Electrochemical Ammonia Synthesis—The Selectivity Challenge. *ACS Catal.* **2017**, *7* (1), 706−709.
(31) Burford, R. J.; Fryzuk, M. D. Examining the Relationship between Coordination Mode and Reactivity of Dinitrogen. *Nat. Rev. Chem.* **2017**, *1* (4), 0026.
(32) Hidai, M.; Mizobe, Y. Recent Advances in the Chemistry of Dinitrogen Complexes. *Chem. Rev.* **1995**, *95* (4), 1115−1133.
(33) Weare, W. W.; Dai, X.; Byrnes, M. J.; Chin, J. M.; Schrock, R. R.; Müller, P. Catalytic Reduction of Dinitrogen to Ammonia at a Single Molybdenum Center. *Proc. Natl. Acad. Sci. U. S. A.* **2006**, *103* (46), 17099−17106.
(34) Zhang, L.; Cong, M.; Ding, X.; Jin, Y.; Xu, F.; Wang, Y.; Chen, L.; Zhang, L. A Janus Fe-SnO_2 Catalyst Enables Bifunctional Electrochemical Nitrogen Fixation, Angew. *Angew. Chem.* **2020**, *132* (27), 10980−10985.
(35) Jiao, Y.; Zheng, Y.; Davey, K.; Qiao, S.-Z. Activity Origin and Catalyst Design Principles for Electrocatalytic Hydrogen Evolution on Heteroatom-Doped Graphene. *Nature Energy* **2016**, *1* (10), 16130.
(36) Guo, C.; Ran, J.; Vasileff, A.; Qiao, S.-Z. Rational Design of Electrocatalysts and Photo(electro)catalysts for Nitrogen Reduction to Ammonia (NH_3) under Ambient Conditions. *Energy Environ. Sci.* **2018**, *11* (1), 45−56.
(37) Cui, X.; Tang, C.; Zhang, Q. A Review of Electrocatalytic Reduction of Dinitrogen to Ammonia under Ambient Conditions. *Adv. Energy. Mater.* **2018**, *8* (22), 1800369.
(38) Giddey, S.; Badwal, S. P. S.; Kulkarni, A. Review of Electrochemical Ammonia Production Technologies and Materials. *Int. J. Hydrogen Energy* **2013**, *38* (34), 14576−14594.
(39) Frank, B.; Blume, R.; Rinaldi, A.; Trunschke, A.; Schlogl, R. Oxygen Insertion Catalysis by sp^2 Carbon. *Angew. Chem., Int. Ed.* **2011**, *50* (43), 10226−10230.
(40) Su, D. S.; Perathoner, S.; Centi, G. Nanocarbons for the Development of Advanced Catalysts. *Chem. Rev.* **2013**, *113* (8), 5782−5816.
(41) Su, D. S.; Zhang, J.; Frank, B.; Thomas, A.; Wang, X.; Paraknowitsch, J.; Schlogl, R. Metal-Free Heterogeneous Catalysis for Sustainable Chemistry. *ChemSusChem* **2010**, *3* (2), 169−180.
(42) Dai, L. Metal-Free Carbon Electrocatalysts: Recent Advances and Challenges Ahead. *Adv. Mater.* **2019**, *31* (13), 1900973.
(43) Zhang, L.-H.; Shi, Y.; Wang, Y.; Shiju, N. R. Nanocarbon Catalysts: Recent Understanding Regarding the Active Sites. *Adv. Sci.* **2020**, *7* (5), 1902126.
(44) Wang, W.; Jia, Q.; Mukerjee, S.; Chen, S. Recent Insights into the Oxygen-Reduction Electrocatalysis of Fe/N/C Materials. *ACS Catal.* **2019**, *9* (11), 10126−10141.
(45) Zhang, G.; Jia, Y.; Zhang, C.; Xiong, X.; Sun, K.; Chen, R.; Chen, W.; Kuang, Y.; Zheng, L.; Tang, H.; Liu, W.; Liu, J.; Sun, X.; Lin, W.-F.; Dai, H. A General Route via Formamide Condensation to Prepare Atomically Dispersed Metal-Nitrogen-Carbon Electrocatalysts for Energy Technologies. *Energy Environ. Sci.* **2019**, *12* (4), 1317−1325.
(46) Sultan, S.; Tiwari, J. N.; Singh, A. N.; Zhumagali, S.; Ha, M.; Myung, C. W.; Thangavel, P.; Kim, K. S. Single Atoms and Clusters Based Nanomaterials for Hydrogen Evolution, Oxygen Evolution Reactions, and Full Water Splitting. *Adv. Energy Mater.* **2019**, *9* (22), 1900624.
(47) Zhu, C.; Shi, Q.; Feng, S.; Du, D.; Lin, Y. Single-Atom Catalysts for Electrochemical Water Splitting. *ACS Energy Lett.* **2018**, *3* (7), 1713−1721.
(48) Soloveichik, G. Electrochemical Synthesis of Ammonia as a Potential Alternative to the Haber-Bosch Process. *Nat. Catal.* **2019**, *2* (5), 377−380.
(49) Jia, H.-P.; Quadrelli, E. A. Mechanistic Aspects of Dinitrogen Cleavage and Hydrogenation to Produce Ammonia in Catalysis and Organometallic Chemistry: Relevance of Metal Hydride Bonds and Dihydrogen. *Chem. Soc. Rev.* **2014**, *43* (2), 547−564.
(50) Zhan, C.-G.; Nichols, J. A.; Dixon, D. A. Ionization Potential, Electron Affinity, Electronegativity, Hardness, and Electron Excitation Energy: Molecular Properties from Density Functional Theory Orbital Energies. *J. Phys. Chem. A* **2003**, *107* (20), 4184−4195.
(51) Deng, J.; Iñiguez, J. A.; Liu, C. Electrocatalytic Nitrogen Reduction at Low Temperature. *Joule* **2018**, *2* (5), 846−856.
(52) Bratsch, S. G. Standard Electrode Potentials and Temperature Coefficients in Water at 298.15 K. *J. Phys. Chem. Ref. Data* **1989**, *18* (1), 1−21.
(53) Bauer, N. Theroetical Pathways for the Reduction of N_2 Molecules in Aqueous Media: Thermodynamics of N_2H_n[1]. *J. Phys. Chem.* **1960**, *64* (7), 833−837.
(54) Koper, M. T. M. Theory of Multiple Proton-Electron Transfer Reactions and Its Implications for Electrocatalysis. *Chem. Sci.* **2013**, *4* (7), 2710−2723.
(55) Gao, K.; Wang, B.; Tao, L.; Cunning, B. V.; Zhang, Z.; Wang, S.; Ruoff, R. S.; Qu, L. Efficient Metal-Free Electrocatalysts from N-Doped Carbon Nanomaterials: Mono-Doping and Co-Doping. *Adv. Mater.* **2019**, *31* (13), 1805121.
(56) Vasileff, A.; Zheng, Y.; Qiao, S. Z. Carbon Solving Carbon's Problems: Recent Progress of Nanostructured Carbon-Based Catalysts for the Electrochemical Reduction of CO_2. *Adv. Energy Mater.* **2017**, *7* (21), 1700759.
(57) Wang, X.; Zhao, Q.; Yang, B.; Li, Z.; Bo, Z.; Lam, K. H.; Adli, N. M.; Lei, L.; Wen, Z.; Wu, G.; Hou, Y. Emerging Nanostructured Carbon-Based Non-Precious Metal Electrocatalysts for Selective Electrochemical CO_2 Reduction to CO. *J. Mater. Chem. A* **2019**, *7* (44), 25191−25202.
(58) Quílez-Bermejo, J.; Morallón, E.; Cazorla-Amorós, D. Metal-Free Heteroatom-Doped Carbon-Based Catalysts for ORR: A Critical Assessment about the role of Heteroatoms. *Carbon* **2020**, *165*, 434−454.
(59) Liang, J.; Jiao, Y.; Jaroniec, M.; Qiao, S. Z. Sulfur and Nitrogen Dual-Doped Mesoporous Graphene Electrocatalyst for Oxygen

https://doi.org/10.1021/acssuschemeng.1c00575
ACS Sustainable Chem. Eng. 2021, 9, 7687−7703

Reduction with Synergistically Enhanced Performance. *Angew. Chem., Int. Ed.* **2012**, *51* (46), 11496−11500.
(60) Zhao, S.; Lu, X.; Wang, L.; Gale, J.; Amal, R. Carbon-Based Metal-Free Catalysts for Electrocatalytic Reduction of Nitrogen for Synthesis of Ammonia at Ambient Conditions. *Adv. Mater.* **2019**, *31* (13), 1805367.
(61) Yuan, L.-P.; Wu, Z.-Y.; Jiang, W.-J.; Tang, T.; Niu, S.; Hu, J.-S. Phosphorus-Doping Activates Carbon Nanotubes for Efficient Electroreduction of Nitrogen to Ammonia. *Nano Res.* **2020**, *13* (5), 1376−1382.
(62) Wu, T.; Li, X.; Zhu, X.; Mou, S.; Luo, Y.; Shi, X.; Asiri, A. M.; Zhang, Y.; Zheng, B.; Zhao, H.; Sun, X. P-Doped Graphene toward Enhanced Electrocatalytic N_2 Reduction. *Chem. Commun.* **2020**, *56* (12), 1831−1834.
(63) Wang, M.; Liu, S.; Ji, H.; Liu, J.; Yan, C.; Qian, T. Unveiling the Essential Nature of Lewis Basicity in Thermodynamically and Dynamically Promoted Nitrogen Fixation. *Adv. Funct. Mater.* **2020**, *30* (32), 2001244.
(64) Zhao, Y.; Hu, C.; Hu, Y.; Cheng, H.; Shi, G.; Qu, L. A Versatile, Ultralight, Nitrogen-Doped Graphene Framework. *Angew. Chem., Int. Ed.* **2012**, *51* (45), 11371−11375.
(65) Ye, L.; Ying, Y.; Sun, D.; Zhang, Z.; Fei, L.; Wen, Z.; Qiao, J.; Huang, H. Highly Efficient Porous Carbon Electrocatalyst with Controllable N-Species Content for Selective CO_2 Reduction. *Angew. Chem., Int. Ed.* **2020**, *59* (8), 3244−3251.
(66) Song, Y.; Chen, W.; Zhao, C.; Li, S.; Wei, W.; Sun, Y. Metal-Free Nitrogen-Doped Mesoporous Carbon for Electroreduction of CO_2 to Ethanol. *Angew. Chem., Int. Ed.* **2017**, *56* (36), 10840−10844.
(67) Li, Q.; Zhang, S.; Dai, L.; Li, L.-s. Nitrogen-Doped Colloidal Graphene Quantum Dots and Their Size-Dependent Electrocatalytic Activity for the Oxygen Reduction Reaction. *J. Am. Chem. Soc.* **2012**, *134* (46), 18932−18935.
(68) Liu, Y.; Su, Y.; Quan, X.; Fan, X.; Chen, S.; Yu, H.; Zhao, H.; Zhang, Y.; Zhao, J. Facile Ammonia Synthesis from Electrocatalytic N_2 Reduction under Ambient Conditions on N-Doped Porous Carbon. *ACS Catal.* **2018**, *8* (2), 1186−1191.
(69) Mukherjee, S.; Cullen, D. A.; Karakalos, S.; Liu, K.; Zhang, H.; Zhao, S.; Xu, H.; More, K. L.; Wang, G.; Wu, G. Metal-Organic Framework-Derived Nitrogen-Doped Highly Disordered Carbon for Electrochemical Ammonia Synthesis using N_2 and H_2O in Alkaline Electrolytes. *Nano Energy* **2018**, *48*, 217−226.
(70) Zhao, C.; Zhang, S.; Han, M.; Zhang, X.; Liu, Y.; Li, W.; Chen, C.; Wang, G.; Zhang, H.; Zhao, H. Ambient Electrosynthesis of Ammonia on a Biomass-Derived Nitrogen-Doped Porous Carbon Electrocatalyst: Contribution of Pyridinic Nitrogen. *ACS Energy Lett.* **2019**, *4* (2), 377−383.
(71) Wang, H.; Wang, L.; Wang, Q.; Ye, S.; Sun, W.; Shao, Y.; Jiang, Z.; Qiao, Q.; Zhu, Y.; Song, P.; Li, D.; He, L.; Zhang, X.; Yuan, J.; Wu, T.; Ozin, G. A. Ambient Electrosynthesis of Ammonia: Electrode Porosity and Composition Engineering, Angew. *Angew. Chem., Int. Ed.* **2018**, *57* (28), 12360−12364.
(72) Song, Y.; Johnson, D.; Peng, R.; Hensley, D. K.; Bonnesen, P. V.; Liang, L.; Huang, J.; Yang, F.; Zhang, F.; Qiao, R.; Baddorf, A. P.; Tschaplinski, T. J.; Engle, N. L.; Hatzell, M. C.; Wu, Z.; Cullen, D. A.; Meyer, H. M.; Sumpter, B. G.; Rondinone, A. J. A Physical Catalyst for the Electrolysis of Nitrogen to Ammonia. *Sci. Adv.* **2018**, *4* (4), 1700336.
(73) Liu, B.; Zheng, Y.; Peng, H.-Q.; Ji, B.; Yang, Y.; Tang, Y.; Lee, C.-S.; Zhang, W. Nanostructured and Boron-Doped Diamond as an Electrocatalyst for Nitrogen Fixation. *ACS Energy Lett.* **2020**, *5* (8), 2590−2596.
(74) Zafari, M.; Kumar, D.; Umer, M.; Kim, K. S. Machine Learning-Based High Throughput Screening for Nitrogen Fixation on Boron-Doped Single Atom Catalysts. *J. Mater. Chem. A* **2020**, *8* (10), 5209−5216.
(75) Liu, C.; Li, Q.; Wu, C.; Zhang, J.; Jin, Y.; MacFarlane, D. R.; Sun, C. Single-Boron Catalysts for Nitrogen Reduction Reaction. *J. Am. Chem. Soc.* **2019**, *141* (7), 2884−2888.
(76) Hering-Junghans, C. Metal-Free Nitrogen Fixation at Boron. *Angew. Chem., Int. Ed.* **2018**, *57* (23), 6738−6740.
(77) Légaré, M.-A.; Bélanger-Chabot, G.; Dewhurst, R. D.; Welz, E.; Krummenacher, I.; Engels, B.; Braunschweig, H. Nitrogen Fixation and Reduction at Boron. *Science* **2018**, *359* (6378), 896.
(78) Yu, X.; Han, P.; Wei, Z.; Huang, L.; Gu, Z.; Peng, S.; Ma, J.; Zheng, G. Boron-Doped Graphene for Electrocatalytic N_2 Reduction. *Joule* **2018**, *2* (8), 1610−1622.
(79) Wang, T.; Xia, L.; Yang, J.-J.; Wang, H.; Fang, W.-H.; Chen, H.; Tang, D.; Asiri, A. M.; Luo, Y.; Cui, G.; Sun, X. Electrocatalytic N_2-to-NH_3 Conversion using Oxygen-Doped Graphene: Experimental and Theoretical Studies. *Chem. Commun.* **2019**, *55* (52), 7502−7505.
(80) Zhao, J.; Wang, B.; Zhou, Q.; Wang, H.; Li, X.; Chen, H.; Wei, Q.; Wu, D.; Luo, Y.; You, J.; Gong, F.; Sun, X. Efficient Electrohydrogenation of N_2 to NH_3 by Oxidized Carbon Nanotubes Under Ambient Conditions. *Chem. Commun.* **2019**, *55* (34), 4997−5000.
(81) Xia, L.; Yang, J.; Wang, H.; Zhao, R.; Chen, H.; Fang, W.; Asiri, A. M.; Xie, F.; Cui, G.; Sun, X. Sulfur-Doped Graphene for Efficient Electrocatalytic N_2-to-NH_3 Fixation. *Chem. Commun.* **2019**, *55* (23), 3371−3374.
(82) Wang, J.; Wang, S.; Li, J. S-Doped Three-Dimensional Graphene (S-3DG): A Metal-Free Electrocatalyst for the Electrochemical Synthesis of Ammonia under Ambient Conditions. *Dalt. Trans.* **2020**, *49* (7), 2258−2263.
(83) Xia, L.; Wu, X.; Wang, Y.; Niu, Z.; Liu, Q.; Li, T.; Shi, X.; Asiri, A. M.; Sun, X. S-Doped Carbon Nanospheres: An Efficient Electrocatalyst toward Artificial N_2 Fixation to NH_3. *Small Methods* **2019**, *3* (6), 1800251.
(84) Yang, Y.; Zhang, L.; Hu, Z.; Zheng, Y.; Tang, C.; Chen, P.; Wang, R.; Qiu, K.; Mao, J.; Ling, T.; Qiao, S.-Z. The Crucial Role of Charge Accumulation and Spin Polarization in Activating Carbon-Based Catalysts for Electrocatalytic Nitrogen Reduction. *Angew. Chem., Int. Ed.* **2020**, *59* (11), 4525−4531.
(85) Liu, Y.; Li, Q.; Guo, X.; Kong, X.; Ke, J.; Chi, M.; Li, Q.; Geng, Z.; Zeng, J. A Highly Efficient Metal-Free Electrocatalyst of F-Doped Porous Carbon toward N_2 Electroreduction. *Adv. Mater.* **2020**, *32* (24), 1907690.
(86) Zhao, J.; Yang, J.; Ji, L.; Wang, H.; Chen, H.; Niu, Z.; Liu, Q.; Li, T.; Cui, G.; Sun, X. Defect-Rich Fluorographene Nanosheets for Artificial N_2 Fixation under Ambient Conditions. *Chem. Commun.* **2019**, *55* (29), 4266−4269.
(87) Zou, H.; Rong, W.; Long, B.; Ji, Y.; Duan, L. Corrosion-Induced Cl-Doped Ultrathin Graphdiyne toward Electrocatalytic Nitrogen Reduction at Ambient Conditions. *ACS Catal.* **2019**, *9* (12), 10649−10655.
(88) Pan, F.; Li, B.; Deng, W.; Du, Z.; Gang, Y.; Wang, G.; Li, Y. Promoting Electrocatalytic CO_2 Reduction on Nitrogen-Doped Carbon with Sulfur Addition. *Appl. Catal., B* **2019**, *252*, 240−249.
(89) Chen, C.; Sun, X.; Yan, X.; Wu, Y.; Liu, H.; Zhu, Q.; Bediako, B. B. A.; Han, B. Boosting CO_2 Electroreduction on N, P-Co-doped Carbon Aerogels. *Angew. Chem., Int. Ed.* **2020**, *59* (27), 11123−11129.
(90) Han, H.; Park, S.; Jang, D.; Lee, S.; Kim, W. B. Electrochemical Reduction of CO_2 to CO by N, S Dual-Doped Carbon Nanoweb Catalysts. *ChemSusChem* **2020**, *13* (3), 539−547.
(91) Zong, L.; Wu, W.; Liu, S.; Yin, H.; Chen, Y.; Liu, C.; Fan, K.; Zhao, X.; Chen, X.; Wang, F.; Yang, Y.; Wang, L.; Feng, S. Metal-Free, Active Nitrogen-Enriched, Efficient Bifunctional Oxygen Electrocatalyst for Ultrastable Zinc-air Batteries. *Energy Storage Materials* **2020**, *27*, 514−521.
(92) Chen, C.; Yan, D.; Wang, Y.; Zhou, Y.; Zou, Y.; Li, Y.; Wang, S. B/N Pairs Enriched Defective Carbon Nanosheets for Ammonia Synthesis with High Efficiency. *Small* **2019**, *15* (7), 1805029.
(93) Kong, Y.; Li, Y.; Yang, B.; Li, Z.; Yao, Y.; Lu, J.; Lei, L.; Wen, Z.; Shao, M.; Hou, Y. Boron and Nitrogen Co-doped Porous Carbon Nanofibers as Metal-free Electrocatalysts for Highly Efficient Ammonia Electrosynthesis. *J. Mater. Chem. A* **2019**, *7* (46), 26272−26278.

https://doi.org/10.1021/acssuschemeng.1c00575
ACS Sustainable Chem. Eng. 2021, 9, 7687−7703

(94) Xiao, S.; Luo, F.; Hu, H.; Yang, Z. Boron and Nitrogen Dual-doped Carbon Nanospheres for Efficient Electrochemical Reduction of N_2 to NH_3. *Chem. Commun.* **2020**, *56* (3), 446−449.
(95) Wang, X.; Vasileff, A.; Jiao, Y.; Zheng, Y.; Qiao, S.-Z. Electronic and Structural Engineering of Carbon-Based Metal-Free Electrocatalysts for Water Splitting. *Adv. Mater.* **2019**, *31* (13), 1803625.
(96) Holmberg, N.; Laasonen, K. Theoretical Insight into the Hydrogen Evolution Activity of Open-Ended Carbon Nanotubes. *J. Phys. Chem. Lett.* **2015**, *6* (19), 3956−3960.
(97) Shen, A.; Zou, Y.; Wang, Q.; Dryfe, R. A. W.; Huang, X.; Dou, S.; Dai, L.; Wang, S. Oxygen Reduction Reaction in a Droplet on Graphite: Direct Evidence that the Edge Is More Active than the Basal Plane. *Angew. Chem., Int. Ed.* **2014**, *53* (40), 10804−10808.
(98) Jia, Y.; Zhang, L.; Du, A.; Gao, G.; Chen, J.; Yan, X.; Brown, C. L.; Yao, X. Defect Graphene as a Trifunctional Catalyst for Electrochemical Reactions. *Adv. Mater.* **2016**, *28* (43), 9532−9538.
(99) Chen, Y.; Wang, Y.; Zhu, S.; Fu, K.; Han, X.; Wang, Y.; Zhao, B.; Li, T.; Liu, B.; Li, Y.; Dai, J.; Xie, H.; Li, T.; Connell, J. W.; Lin, Y.; Hu, L. Nanomanufacturing of Graphene Nanosheets through Nanohole Opening and Closing. *Mater. Today* **2019**, *24*, 26−32.
(100) Dou, S.; Xu, J.; Cui, X.; Liu, W.; Zhang, Z.; Deng, Y.; Hu, W.; Chen, Y. High-Temperature Shock Enabled Nanomanufacturing for Energy-Related Applications. *Adv. Energy Mater.* **2020**, *10*, 2001331.
(101) Zhang, M.; Choi, C.; Huo, R.; Gu, G. H.; Hong, S.; Yan, C.; Xu, S.; Robertson, A. W.; Qiu, J.; Jung, Y.; Sun, Z. Reduced Graphene Oxides with Engineered Defects Enable Efficient Electrochemical Reduction of Dinitrogen to Ammonia in Wide pH Range. *Nano Energy* **2020**, *68*, 104323.
(102) Chen, S.; Zhao, L.; Ma, J.; Wang, Y.; Dai, L.; Zhang, J. Edge-Doping Modulation of N, P-codoped Porous Carbon Spheres for High-Performance Rechargeable Zn-air Batteries. *Nano Energy* **2019**, *60*, 536−544.
(103) Lv, C.; Qian, Y.; Yan, C.; Ding, Y.; Liu, Y.; Chen, G.; Yu, G. Defect Engineering Metal-Free Polymeric Carbon Nitride Electrocatalyst for Effective Nitrogen Fixation under Ambient Conditions. *Angew. Chem., Int. Ed.* **2018**, *57* (32), 10246−10250.
(104) Peng, G.; Wu, J.; Wang, M.; Niklas, J.; Zhou, H.; Liu, C. Nitrogen-Defective Polymeric Carbon Nitride Nanolayer Enabled Efficient Electrocatalytic Nitrogen Reduction with High Faradaic Efficiency. *Nano Lett.* **2020**, *20* (4), 2879−2885.
(105) Yandulov, D. V.; Schrock, R. R. Reduction of Dinitrogen to Ammonia at a Well-Protected Reaction Site in a Molybdenum Triamidoamine Complex. *J. Am. Chem. Soc.* **2002**, *124* (22), 6252−6253.
(106) Yandulov, D. V.; Schrock, R. R. Catalytic Reduction of Dinitrogen to Ammonia at a Single Molybdenum Center. *Science* **2003**, *301* (5629), 76.
(107) Arashiba, K.; Miyake, Y.; Nishibayashi, Y. A Molybdenum Complex Bearing PNP-type Pincer Ligands Leads to the Catalytic Reduction of Dinitrogen into Ammonia. *Nat. Chem.* **2011**, *3* (2), 120−125.
(108) Anderson, J. S.; Rittle, J.; Peters, J. C. Catalytic Conversion of Nitrogen to Ammonia by an Iron Model Complex. *Nature* **2013**, *501* (7465), 84−87.
(109) Zahran, Z. N.; Tsubonouchi, Y.; Mohamed, E. A.; Yagi, M. Recent Advances in the Development of Molecular Catalyst-Based Anodes for Water Oxidation toward Artificial Photosynthesis. *ChemSusChem* **2019**, *12* (9), 1775−1793.
(110) Wang, A.; Li, J.; Zhang, T. Heterogeneous Single-Atom Catalysis. *Nat. Rev. Chem.* **2018**, *2* (6), 65−81.
(111) Chen, Y.; Ji, S.; Chen, C.; Peng, Q.; Wang, D.; Li, Y. Single-Atom Catalysts: Synthetic Strategies and Electrochemical Applications. *Joule* **2018**, *2* (7), 1242−1264.
(112) Nguyen, T. N.; Salehi, M.; Le, Q. V.; Seifitokaldani, A.; Dinh, C. T. Fundamentals of Electrochemical CO_2 Reduction on Single-Metal-Atom Catalysts. *ACS Catal.* **2020**, *10* (17), 10068−10095.
(113) Han, A.; Wang, B.; Kumar, A.; Qin, Y.; Jin, J.; Wang, X.; Yang, C.; Dong, B.; Jia, Y.; Liu, J.; Sun, X. Recent Advances for MOF-Derived Carbon-Supported Single-Atom Catalysts. *Small Methods* **2019**, *3* (9), 1800471.
(114) Su, J.; Ge, R.; Dong, Y.; Hao, F.; Chen, L. Recent Progress in Single-Atom Electrocatalysts: Concept, Synthesis, and Applications in Clean Energy Conversion. *J. Mater. Chem. A* **2018**, *6* (29), 14025−14042.
(115) Zhang, Q.; Guan, J. Single-Atom Catalysts for Electrocatalytic Applications. *Adv. Funct. Mater.* **2020**, *30* (31), 2000768.
(116) Zhang, H.; Tian, W.; Duan, X.; Sun, H.; Liu, S.; Wang, S. Catalysis of a Single Transition Metal Site for Water Oxidation: From Mononuclear Molecules to Single Atoms. *Adv. Mater.* **2020**, *32* (18), 1904037.
(117) Liu, J.; Kong, X.; Zheng, L.; Guo, X.; Liu, X.; Shui, J. Rare Earth Single-Atom Catalysts for Nitrogen and Carbon Dioxide Reduction. *ACS Nano* **2020**, *14* (1), 1093−1101.
(118) Zhai, Y.; Zhu, Z.; Zhu, C.; Chen, K.; Zhang, X.; Tang, J.; Chen, J. Single-atom catalysts boost nitrogen electroreduction reaction. *Mater. Today* **2020**, *38*, 99.
(119) Zhai, G.-Y.; Xu, D.; Zhang, S.-N.; Xue, Z.-H.; Su, H.; Yu, Q.-Y.; Wang, H.-H.; Lin, X.; Lin, Y.-X.; Sun, L.-H.; Li, X.-H.; Chen, J.-S. Isoelectric Si Heteroatoms as Electron Traps for N_2 Fixation and Activation. *Adv. Funct. Mater.* **2020**, *30* (51), 2005779.
(120) Ling, C.; Bai, X.; Ouyang, Y.; Du, A.; Wang, J. Single Molybdenum Atom Anchored on N-Doped Carbon as a Promising Electrocatalyst for Nitrogen Reduction into Ammonia at Ambient Conditions. *J. Phys. Chem. C* **2018**, *122* (29), 16842−16847.
(121) Zhang, L.; Zhao, W.; Zhang, W.; Chen, J.; Hu, Z. g-C_3N_4 Coordinated Single Atom as an Efficient Electrocatalyst for Nitrogen Reduction Reaction. *Nano Res.* **2019**, *12* (5), 1181−1186.
(122) Ling, C.; Ouyang, Y.; Li, Q.; Bai, X.; Mao, X.; Du, A.; Wang, J. A General Two-Step Strategy-Based High-Throughput Screening of Single Atom Catalysts for Nitrogen Fixation. *Small Methods* **2019**, *3* (9), 1800376.
(123) Li, X.-F.; Li, Q.-K.; Cheng, J.; Liu, L.; Yan, Q.; Wu, Y.; Zhang, X.-H.; Wang, Z.-Y.; Qiu, Q.; Luo, Y. Conversion of Dinitrogen to Ammonia by FeN_3-Embedded Graphene. *J. Am. Chem. Soc.* **2016**, *138* (28), 8706−8709.
(124) Guo, X.; Gu, J.; Lin, S.; Zhang, S.; Chen, Z.; Huang, S. Tackling the Activity and Selectivity Challenges of Electrocatalysts toward the Nitrogen Reduction Reaction via Atomically Dispersed Biatom Catalysts. *J. Am. Chem. Soc.* **2020**, *142* (12), 5709−5721.
(125) Liu, X.; Jiao, Y.; Zheng, Y.; Jaroniec, M.; Qiao, S.-Z. Building Up a Picture of the Electrocatalytic Nitrogen Reduction Activity of Transition Metal Single-Atom Catalysts. *J. Am. Chem. Soc.* **2019**, *141* (24), 9664−9672.
(126) Azofra, L. M.; Sun, C.; Cavallo, L.; MacFarlane, D. R. Feasibility of N_2 Binding and Reduction to Ammonia on Fe-Deposited MoS_2 2D Sheets: A DFT Study. *Chem. - Eur. J.* **2017**, *23* (34), 8275−8279.
(127) Wang, Z.; Yu, Z.; Zhao, J. Computational Screening of a Single Transition Metal Atom Supported on the C_2N Monolayer for Electrochemical Ammonia Synthesis. *Phys. Chem. Chem. Phys.* **2018**, *20* (18), 12835−12844.
(128) Zhao, J.; Zhao, J.; Cai, Q. Single Transition Metal Atom Embedded into a MoS_2 Nanosheet as a Promising Catalyst for Electrochemical Ammonia Synthesis. *Phys. Chem. Chem. Phys.* **2018**, *20* (14), 9248−9255.
(129) Cao, Y.; Gao, Y.; Zhou, H.; Chen, X.; Hu, H.; Deng, S.; Zhong, X.; Zhuang, G.; Wang, J. Highly Efficient Ammonia Synthesis Electrocatalyst: Single Ru Atom on Naturally Nanoporous Carbon Materials. *Adv. Theory Simul.* **2018**, *1* (5), 1800018.
(130) Tao, H.; Choi, C.; Ding, L.-X.; Jiang, Z.; Han, Z.; Jia, M.; Fan, Q.; Gao, Y.; Wang, H.; Robertson, A. W.; Hong, S.; Jung, Y.; Liu, S.; Sun, Z. Nitrogen Fixation by Ru Single-Atom Electrocatalytic Reduction. *Chem.* **2019**, *5* (1), 204−214.
(131) Geng, Z.; Liu, Y.; Kong, X.; Li, P.; Li, K.; Liu, Z.; Du, J.; Shu, M.; Si, R.; Zeng, J. N_2 Electrochemical Reduction: Achieving a Record-High Yield Rate of 120.9 $\mu g_{NH3} mg_{cat}^{-1} h^{-1}$ for N_2 Electro-

https://doi.org/10.1021/acssuschemeng.1c00575
ACS Sustainable Chem. Eng. 2021, 9, 7687−7703

chemical Reduction over Ru Single-Atom Catalysts. *Adv. Mater.* **2018**, *30* (40), 1870301.
(132) Yu, B.; Li, H.; White, J.; Donne, S.; Yi, J.; Xi, S.; Fu, Y.; Henkelman, G.; Yu, H.; Chen, Z.; Ma, T. Tuning the Catalytic Preference of Ruthenium Catalysts for Nitrogen Reduction by Atomic Dispersion. *Adv. Funct. Mater.* **2020**, *30* (6), 1905665.
(133) Wang, X.; Wang, W.; Qiao, M.; Wu, G.; Chen, W.; Yuan, T.; Xu, Q.; Chen, M.; Zhang, Y.; Wang, X.; Wang, J.; Ge, J.; Hong, X.; Li, Y.; Wu, Y.; Li, Y. Atomically Dispersed Au1 Catalyst towards Efficient Electrochemical Synthesis of Ammonia. *Sci. Bull.* **2018**, *63* (19), 1246−1253.
(134) Qin, Q.; Heil, T.; Antonietti, M.; Oschatz, M. Single-Site Gold Catalysts on Hierarchical N-Doped Porous Noble Carbon for Enhanced Electrochemical Reduction of Nitrogen. *Small Methods* **2018**, *2* (12), 1800202.
(135) Burgess, B. K.; Lowe, D. J. Mechanism of Molybdenum Nitrogenase. *Chem. Rev.* **1996**, *96* (7), 2983−3012.
(136) Han, L.; Liu, X.; Chen, J.; Lin, R.; Liu, H.; Lü, F.; Bak, S.; Liang, Z.; Zhao, S.; Stavitski, E.; Luo, J.; Adzic, R. R.; Xin, H. L. Atomically Dispersed Molybdenum Catalysts for Efficient Ambient Nitrogen Fixation. *Angew. Chem., Int. Ed.* **2019**, *58* (8), 2321.
(137) Kärkäs, M. D.; Åkermark, B. Water Oxidation using Earth-abundant Transition Metal Catalysts: Opportunities and Challenges. *Dalt. Trans.* **2016**, *45* (37), 14421−14461.
(138) Zhang, W.; Lai, W.; Cao, R. Energy-Related Small Molecule Activation Reactions: Oxygen Reduction and Hydrogen and Oxygen Evolution Reactions Catalyzed by Porphyrin- and Corrole-Based Systems. *Chem. Rev.* **2017**, *117* (4), 3717−3797.
(139) Wang, J.; Cui, W.; Liu, Q.; Xing, Z.; Asiri, A. M.; Sun, X. Recent Progress in Cobalt-Based Heterogeneous Catalysts for Electrochemical Water Splitting. *Adv. Mater.* **2016**, *28* (2), 215−230.
(140) Gewirth, A. A.; Varnell, J. A.; DiAscro, A. M. Nonprecious Metal Catalysts for Oxygen Reduction in Heterogeneous Aqueous Systems. *Chem. Rev.* **2018**, *118* (5), 2313−2339.
(141) Yu, F.; Li, F.; Hu, J.; Bai, L.; Zhu, Y.; Sun, L. Electrocatalytic Water Oxidation by a Macrocyclic Cu(ii) Complex in Neutral Phosphate Buffer. *Chem. Commun.* **2016**, *52* (68), 10377−10380.
(142) Zhang, L.-H.; Yu, F.; Shi, Y.; Li, F.; Li, H. Base-Enhanced Electrochemical Water Oxidation by a Nickel Complex in Neutral Aqueous Solution. *Chem. Commun.* **2019**, *55* (43), 6122−6125.
(143) Yu, F.; Li, F.; Zhang, B.; Li, H.; Sun, L. Efficient Electrocatalytic Water Oxidation by a Copper Oxide Thin Film in Borate Buffer. *ACS Catal.* **2015**, *5* (2), 627−630.
(144) Yu, F.; Li, F.; Yao, T.; Du, J.; Liang, Y.; Wang, Y.; Han, H.; Sun, L. Fabrication and Kinetic Study of a Ferrihydrite-Modified $BiVO_4$ Photoanode. *ACS Catal.* **2017**, *7* (3), 1868−1874.
(145) Zhang, W.; Yang, S.; Bai, S.-T.; Zhang, L.-H.; Zhang, Y.; Yu, F. Heterogenization of Ionic liquid Boosting Electrochemical Oxygen Reduction Performance of Co_3O_4 Supported on Graphene Oxide. *ChemCatChem* **2021**, *13* (6), 1546−1551.
(146) Wang, M.; Liu, S.; Qian, T.; Liu, J.; Zhou, J.; Ji, H.; Xiong, J.; Zhong, J.; Yan, C. Over 56.55% Faradaic Efficiency of Ambient Ammonia Synthesis Enabled by Positively Shifting the Reaction Potential. *Nat. Commun.* **2019**, *10* (1), 341.
(147) Lü, F.; Zhao, S.; Guo, R.; He, J.; Peng, X.; Bao, H.; Fu, J.; Han, L.; Qi, G.; Luo, J.; Tang, X.; Liu, X. Nitrogen-Coordinated Single Fe Sites for Efficient Electrocatalytic N_2 Fixation in Neutral Media. *Nano Energy* **2019**, *61*, 420−427.
(148) Zhang, S.; Jin, M.; Shi, T.; Han, M.; Sun, Q.; Lin, Y.; Ding, Z.; Zheng, L. R.; Wang, G.; Zhang, Y.; Zhang, H.; Zhao, H. Electrocatalytically Active Fe-$(O\text{-}C_2)_4$ Single-Atom Sites for Efficient Reduction of Nitrogen to Ammonia. *Angew. Chem., Int. Ed.* **2020**, *59* (32), 13423−13429.
(149) Fang, Y.; Xue, Y.; Li, Y.; Yu, H.; Hui, L.; Liu, Y.; Xing, C.; Zhang, C.; Zhang, D.; Wang, Z.; Chen, X.; Gao, Y.; Huang, B.; Li, Y. Graphdiyne Interface Engineering: Highly Active and Selective Ammonia Synthesis. *Angew. Chem., Int. Ed.* **2020**, *59* (31), 13021−13027.
(150) Gao, Y.; Han, Z.; Hong, S.; Wu, T.; Li, X.; Qiu, J.; Sun, Z. ZIF-67-Derived Cobalt/Nitrogen-Doped Carbon Composites for Efficient Electrocatalytic N_2 Reduction. *ACS Appl. Energy Mater.* **2019**, *2* (8), 6071−6077.
(151) Mukherjee, S.; Yang, X.; Shan, W.; Samarakoon, W.; Karakalos, S.; Cullen, D. A.; More, K.; Wang, M.; Feng, Z.; Wang, G.; Wu, G. Atomically Dispersed Single Ni Site Catalysts for Nitrogen Reduction toward Electrochemical Ammonia Synthesis Using N_2 and H_2O. *Small Methods* **2020**, *4* (6), 1900821.
(152) Li, C.; Mou, S.; Zhu, X.; Wang, F.; Wang, Y.; Qiao, Y.; Shi, X.; Luo, Y.; Zheng, B.; Li, Q.; Sun, X. Dendritic Cu: a High-Efficiency Electrocatalyst for N_2 Fixation to NH_3 under Ambient Conditions. *Chem. Commun.* **2019**, *55* (96), 14474−14477.
(153) Lin, Y.-X.; Zhang, S.-N.; Xue, Z.-H.; Zhang, J.-J.; Su, H.; Zhao, T.-J.; Zhai, G.-Y.; Li, X.-H.; Antonietti, M.; Chen, J.-S. Boosting Selective Nitrogen Reduction to Ammonia on Electron-Deficient Copper Nanoparticles. *Nat. Commun.* **2019**, *10* (1), 4380.
(154) Zang, W.; Yang, T.; Zou, H.; Xi, S.; Zhang, H.; Liu, X.; Kou, Z.; Du, Y.; Feng, Y. P.; Shen, L.; Duan, L.; Wang, J.; Pennycook, S. J. Copper Single Atoms Anchored in Porous Nitrogen-Doped Carbon as Efficient pH-Universal Catalysts for the Nitrogen Reduction Reaction. *ACS Catal.* **2019**, *9* (11), 10166−10173.

https://doi.org/10.1021/acssuschemeng.1c00575
ACS Sustainable Chem. Eng. 2021, 9, 7687−7703